Systems/Circuits

Excitatory Projections from the Prefrontal Cortex to Nucleus Accumbens Core D1-MSNs and κ Opioid Receptor Modulate Itch-Related Scratching Behaviors

Xiao-Bo Wu, Qian Zhu, Ming-Hui Gao, Sheng-Xiang Yan, Pan-Yang Gu, Peng-Fei Zhang, Meng-Lin Xu, and Yong-Jing Gao

Institute of Pain Medicine and Special Environmental Medicine, Co-innovation Center of Neuroregeneration, Nantong University, Jiangsu 226019, China

Itch is an uncomfortable and complex sensation that elicits the desire to scratch. The nucleus accumbens (NAc) activity is important in driving sensation, motivation, and emotion. Excitatory afferents from the medial prefrontal cortex (mPFC), amygdala, and hippocampus are crucial in tuning the activity of dopamine receptor D1-expressing and D2-expressing medium spiny neurons (Drd1-MSN and Drd2-MSN) in the NAc. However, a cell-type and neural circuity-based mechanism of the NAc underlying acute itch remains unclear. We found that acute itch induced by compound 48/80 (C48/80) decreased the intrinsic membrane excitability in Drd1-MSNs, but not in Drd2-MSNs, in the NAc core of male mice. Chemogenetic activation of Drd1-MSNs alleviated C48/80-induced scratching behaviors but not itch-related anxiety-like behaviors. In addition, C48/80 enhanced the frequency of spontaneous EPSCs (sEPSCs) and reduced the paired-pulse ratio (PPR) of electrical stimulation-evoked EPSCs in Drd1-MSNs. Furthermore, C48/80 increased excitatory synaptic afferents to Drd1-MSNs from the mPFC, not from the basolateral amygdala (BLA) or ventral hippocampus (vHipp). Consistently, the intrinsic excitability of mPFC-NAc projecting pyramidal neurons was increased after C48/80 treatment. Chemogenetic inhibition of mPFC-NAc excitatory synaptic afferents relieved the scratching behaviors. Moreover, pharmacological activation of κ opioid receptor (KOR) in the NAc core suppressed C48/80-induced scratching behaviors, and the modulation of KOR activity in the NAc resulted in the changes of presynaptic excitatory inputs to Drd1-MSNs in C48/80-treated mice. Together, these results reveal the neural plasticity in synapses of NAc Drd1-MSNs from the mPFC underlying acute itch and indicate the modulatory role of the KOR in itch-related scratching behaviors.

Key words: **dopamine D1 receptor; itch; κ opioid receptor; medial prefrontal cortex; nucleus accumbens**

Significance Statement

Itch stimuli cause strongly scratching desire and anxiety in patients. However, the related neural mechanisms remain largely unclear. In the present study, we demonstrated that the pruritogen compound 48/80 (C48/80) shapes the excitability of dopamine receptor D1-expressing medium spiny neurons (Drd1-MSNs) in the nucleus accumbens (NAc) core and the glutamatergic synaptic afferents from medial prefrontal cortex (mPFC) to these neurons. Chemogenetic activation of Drd1-MSNs or inhibition of mPFC-NAc excitatory synaptic afferents relieves the scratching behaviors. In addition, pharmacological activation of κ opioid receptor (KOR) in the NAc core alleviates C48/80-induced itch. Thus, targeting mPFC-NAc Drd1-MSNs or KOR may provide effective treatments for itch.

Received July 11, 2022; revised Dec. 28, 2022; accepted Jan. 6, 2023.

Author contributions: X.-B.W. and Y.-J.G. designed research; Q.Z., M.-H.G., S.-X.Y., P.-Y.G., P.-F.Z., and M.-L.X. performed research; Q.Z., S.-X.Y., and P.-Y.G. analyzed data; X.-B.W. and Y.-J.G. wrote the paper.

This work was supported by the STI2030-Major Projects 2022ZD0204700 and National Natural Science Foundation of China (NSFC) Grants 32030048 and 32171000.

The authors declare no competing financial interests.

Correspondence should be addressed to Yong-Jing Gao at gaoyongjing@ntu.edu.cn or Xiao-Bo Wu at xbwu1983@ntu.edu.cn.

https://doi.org/10.1523/JNEUROSCI.1359-22.2023

Copyright © 2023 the authors

Introduction

Itch is a complex and uncomfortable sensation that strongly provokes the desire to scratch. Repeated, excessive scratches cause severe damage to the skin tissue and diminish the quality of life in patients with chronic itch (Murota et al., 2010; Zachariae et al., 2012; Lavery et al., 2016). Human imaging studies showed that scratching is related to the activity of the reward system, including the prefrontal cortex, orbitofrontal cortex, midbrain, and caudate nucleus (Papoiu et al., 2013; Mochizuki et al., 2014, 2015). However, itching also triggers

negative emotions like anxiety and depression (Bartels et al., 2016; Sanders and Akiyama, 2018). Recent studies have identified that neuronal populations in the amygdala are involved in itch-related sensation and negative emotions (Sanders et al., 2019; Samineni et al., 2021). Additionally, the ventral tegmental area (VTA) dopaminergic neurons process the itch-related scratching behavior, while GABAergic neurons are implicated in the itch-induced aversion (Su et al., 2019).

The nucleus accumbens (NAc) is a critical brain region of mesolimbic dopamine circuitry and roughly divided into the core and shell subregions (Zahm and Brog, 1992). The two subregions have distinct anatomic structures and encode relatively different behaviors, but share similar local circuitry (Floresco, 2015). NAc primarily receives excitatory afferents from the medial prefrontal cortex (mPFC), basolateral amygdala (BLA), ventral hippocampus (vHipp), and thalamus that are involved in motivation/desire-related behaviors (Suska et al., 2013; LeGates et al., 2018; Y. Wang et al., 2020; Chisholm et al., 2021). A recent study provide evidence that itch stimuli dynamically regulate dopamine level in the NAc shell region, which is involved in itch-related scratching (Yuan et al., 2018, 2019). In addition, the anterior cingulate cortex and amygdala are activated by itch stimuli (Lu et al., 2018; Sanders et al., 2019; Zhang et al., 2022). These results support the circuitry containing such brain regions may contribute to the itch-related activities. Excitatory synaptic afferents integrate in the NAc medium-sized spiny neurons (MSNs), which are transcriptionally segregated into dopamine D1 receptor-expressing MSNs (Drd1-MSNs) and D2 receptor-expressing MSNs (Drd2-MSNs; Kreitzer, 2009). Previous studies demonstrated that different activities of Drd1- and Drd2-MSNs might code distinct emotional behavior responses (Soares-Cunha et al., 2016). However, the neural circuits and functional roles of the NAc MSN subtypes underlying itch-related scratching and affective components remain unknown.

In the NAc, the κ opioid receptor (KOR) is densely expressed on the presynaptic terminals of dopaminergic and glutamatergic inputs and regulates the release of dopamine and glutamate (Hjelmstad and Fields, 2001; Karkhanis et al., 2016). Activation of KOR in the NAc modulates the response to reward (Chartoff et al., 2016) and aversive stimuli, including pain-induced negative affect (Massaly et al., 2019). Pharmacological studies have shown that KOR agonists are promising therapeutic candidates for intractable itch by their antipruritic effects in both animals and humans (Phan et al., 2012). However, the underlying mechanisms of the antipruritic effects for KOR activation remain elusive. In this study, we investigated the role of MSN subtypes in the NAc core and their excitatory afferent circuits in itch-related behaviors and provided the cellular evidence for KOR modulation on synaptic adaptation in itch signal processing.

Materials and Methods

Animals

All animal procedures performed in this study were reviewed and approved by the Animal Care and Use Committee of Nantong University (Jiangsu, China). Male mice (8–12 weeks) were maintained on a 12/12 h light/dark cycle (lights on at 6:30 A.M.) at room temperature of 22 ± 3°C with free access to food and water. All mice were acclimated to the animal facility for 5–7 d before the initiation of experimental procedures. Drd1a-tdTomato (6Calak/J, catalog #016204, The Jackson Laboratory), Drd2-EGFP (B6.FVB (Cg)-Tg(Drd2-EGFP)S118Gsat/KreMmucd, catalog #036931-UCD, MMRRC), and Drd1a-Cre (Tg(Drd1-cre)EY217Gsat/Mmcd, catalog #030778-UCD, MMRRC) BAC transgenic mice on a C57BL/6J background were used in this study.

Drugs

U50488 was purchased from Tocris Bioscience. Compound 48/80 (C48/80), picrotoxin (PTX), clozapine N-oxide (CNO), norbinaltorphimine (nor-BNI), and the other chemicals were purchased from Sigma-Aldrich.

Brain cannula implantation and drug injection

The animals were anesthetized with isoflurane. Guided cannulas (26 G, RWD Life Science) were implanted above the bilateral NAc (AP: +1.5 mm; lateral: ±0.8 mm; depth: −4.0 mm from the skull). An injection needle (32 G, Hamilton) was inserted through the guide cannula, and drug solution or vehicle (0.3 μl/site) was slowly injected over 5 min. Locations of the cannula placement were confirmed at the time of tissue harvest.

Stereotaxic surgery

For optogenetic manipulation, the mice were anesthetized with isoflurane and immobilized with a stereotaxic frame (RWD Life Science). After a craniotomy was performed, each mouse received a bilateral injection of pAAV9-CamKIIα-ChR2 (H134R)-eYFP (AAV-CaMKIIα-ChR2-eYFP, viral titer 5.2×10^{12} vg/ml; packaged by Shanghai OBiO Technology) into the mPFC (stereotaxic coordinates from bregma: A/P: +1.6 mm, M/L: ±0.4 mm, D/V: −2.5 mm), BLA (A/P: −1.3 mm, M/L: ±2.8 mm, D/V: −4.8 mm), or vHipp (A/P: −3.1 mm, M/L: ±2.9 mm, D/V: −4.5 mm). A total of 0.4–0.6 μl (two sites) of virus solution was infused at a rate of 0.05 μl/min by a syringe pump. The amount of the injection volume is 0.6 μl (0.3 μl/site) into mPFC, 0.4 μl (0.2 μl/site) into BLA, and 0.6 μl (0.3 μl/site) into vHipp. For chemogenetic manipulation, AAV5-Ef1α-DIO-hM3D(Gq)-mCherry (AAV-DIO-hM3Dq-mCherry), AAV5-Ef1α-DIO-hM4D(Gi)-mCherry (AAV-DIO-hM4Di-mCherry), or AAV5-Ef1α-DIO-mCherry (AAV-DIO-mCherry) were bilaterally injected into the NAc core. For chemogenetic inhibition of PFC-NAc synaptic projections, AAV5-CaMKIIα-hM4D(Gi)-mCherry (AAV-CaMKIIα-hM4Di-mCherry) or AAV5-CaMKIIα-mCherry (AAV-CaMKIIα-mCherry) were bilaterally injected into the mPFC (places are same as above), and then the cannulas were implanted into the NAc. After injection, the syringe was left in place for 8–10 min. To identify PFC-NAc projection pyramidal neurons, 0.1 μl/site retrobeads green was bilaterally injected into the NAc core (AP: +1.5 mm; lateral: ±0.8 mm; depth: −4.2 mm from the skull).

Neck model of acute itch

All mice were shaved on the back of neck and then were habituated to the experimenters by handling for 3 d before experiments. For the scratching behavior test, mice were individually placed into small plastic chambers (15 × 15 × 15 cm) on an elevated metal mesh floor and habituated for at least 30 min. After mild anesthesia with isoflurane, mice were injected intradermally with Compound 48/80 (C48/80, 100 μg/50 μl; Sigma-Aldrich) or saline into the rostral back skin. Immediately after the injection, the itch-related scratching behavior was recorded with a video camera for 30 min and the bouts of scratching were assessed. One bout of scratching was counted as a mouse lifting of either hindpaw to scratch the injection site of the shaved skin and then returning it back to the floor or licking/biting of the toes (Jing et al., 2018; Z.H. Wu et al., 2021).

Elevated plus-maze test (EPMT)

The elevated plus-maze (EPM) test (EPMT) apparatus consisted of four arms (30 cm long and 5 cm wide) and was elevated 32 cm from the floor. All mice were acclimated to the testing room 45 min before the initiation of the experiment. After intradermal injection of C48/80 or saline, each mouse was placed back in the home cage for 30 min. After that, each mouse was placed at the center square of the maze, facing the open arm, and allowed to explore the maze for 5 min. The entry into an arm was counted by the presence of all four paws on the floor of that arm. The total time spent in the open arms and the number of entries to these arms were used in the assessment of anxiety-like behavior. The animal behavior parameters were analyzed with a video tracking and analysis

system (ANY-maze software, Stoelting). To eliminate the possible bias, all the arms were equally illuminated and thoroughly cleaned with 75% ethanol after each trial.

Open-field test (OFT)

The open-field (OF) test (OFT) apparatus is composed of a white PVC box (60 × 60 cm, 50 cm in height). The floor was subdivided into 16 equal parts. The central zone was defined by the four squares in the middle field. Same as in the EPM test, each mouse was acclimated to the testing room 45 min before the initiation of the experiment. After intradermal injection of C48/80 or saline, each mouse was placed back in the home cage for 30 min. Then the mouse was put in the middle of the field and was tested individually within a 5-min session. The behavioral data were analyzed by the ANY-maze system (Stoelting Co). The time spent in the central zone and the total travel distance was counted. The inner sides of the apparatus were carefully cleaned with 75% ethanol after each trial.

Brain slices preparation and patch-clamp recording

Brain slice preparation and whole-cell recordings were conducted the same as our published protocol (X.B. Wu et al., 2018). Briefly, 30 min after saline or C48/80 intradermal injection, the mice were anesthetized with isoflurane and decapitated. The brains were quickly removed and immediately immersed into the ice-cold artificial CSF (aCSF). Sucrose-rich aCSF contains 235 mM sucrose, 2.5 mM KCl, 1.25 mM NaH_2PO_4, 1 mM $CaCl_2$, 2.5 mM $MgCl_2$, 25 mM $NaHCO_3$, and 10 mM glucose, oxygenated with 95% O_2 plus 5% CO_2. Coronal brain slices (250 μm) containing the NAc core or PFC region were cut with a vibratome (Series 1000; Leica). Slices were incubated with oxygenated (95% O_2 + 5% CO_2) normal aCSF containing 125 mM NaCl, 3 mM KCl, 1.25 mM NaH_2PO_4, 2.4 mM $CaCl_2$, 1.2 mM $MgCl_2$, 26 mM $NaHCO_3$, and 10 mM glucose for 30 min at 34°C and subsequently stored in room temperature at least 1 h before electrophysiological recording.

Slices were placed in a recording chamber and were continuously perfused with oxygenated normal aCSF. Cells were visualized by an infrared-differential interference contrast (IR-DIC) and fluorescent microscope (BX51WIF, Olympus) equipped with a digital sCMOS camera (optiMOS, QImaging, United States). Whole-cell patch-clamp recordings of NAc core neurons were conducted using a patch-clamp amplifier (Multiclamp 700B; Molecular Devices). Data acquisition was performed by using a digitizer (DigiData 1400A; Molecular Devices) and analyzed with Clampfit 10.4 software (Molecular Devices), respectively. Cells located in the ventral-medial subregion of the NAc core MSNs with tdTomato (Drd1+) or eGFP (Drd2+) were identified by their fluorescence. A typical MSN was further confirmed by its small morphology (somatic diameters, <20 μm) and hyperpolarized resting membrane potential (RMP; hyperpolarize than −75 mV). For PFC-NAc projection pyramidal neurons recording, retrobeads positive cells in the PFC region were identified by their green fluorescence. The patch pipette resistance was 4–8 MΩ when filled with pipette solution, and seal resistances were >1 GΩ. Data were digitized at 10 kHz and low-pass filtered at 2 kHz.

The intrinsic membrane excitability recordings were performed with a pipette solution containing 120 mM K-gluconate, 20 mM KCl, 0.3 mM GTP-Tris, 4 mM Na_2ATP, 10 mM HEPES, 0.2 mM EGTA, and 2 mM $MgCl_2$, pH 7.2–7.4, which adjusted with KOH. After establishing a well whole-cell configuration, recordings were done in the current-clamp model at room temperature (23 ± 1°C). All neuronal excitability measurements were performed at the resting membrane potential (RMP). Only the RMP "stable" (oscillating <3 mV within 5 min) neurons were adopted for the following recordings. A series of step currents (−200 to +200 pA, with a 20-pA increment, pulse duration, 1 s, and interpulse interval, 15 s) were run (at least three runs) to measure the membrane properties. For a recorded neuron, the number of evoked action potentials with a variation >20% (run-down or run-up) were excluded from further data analysis.

To measure the EPSCs, electrodes were filled with a cesium-based internal pipette solution containing 120 mM cesium methanesulfonate, 2 mM NaCl, 20 mM HEPES, 5 mM tetraethylammonium-Cl, 0.4 mM EGTA, 2.5 mM Na_2ATP, 0.3 mM GTP-Tris, and 2.5 mM QX-314, pH 7.2–7.4, which adjusted with CsOH. The spontaneous and evoked EPSCs were recorded at −70 mV in a voltage-clamp model. Spontaneous EPSCs (sEPSCs) were obtained at least 10 min for each recorded cell and $GABA_A$ receptor antagonist picrotoxin (PTX; 100 μM) was present in the aCSF. For sEPSCs analysis, a template was conducted by averaging 80–100 hand-picked spontaneous events with pClamp10.4 software. To measure the role of the κ receptor in excitatory synaptic transmission at the NAc core, miniature EPSCs (mEPSCs) were obtained in the presence of 100 μM PTX and 1 μM TTX. The selective KOR agonist U50488 (1 μM) or selective KOR antagonist nor-BNI (0.1 μM) was added to the aCSF after the basal recording (Mu et al., 2011; Kallupi et al., 2013). Electrical stimulations (produced by Master 8; AMPI Technologies) at 0.1 Hz (pulse of 100-μs duration) by a concentric bipolar electrode (FHC) were used to evoke EPSCs in some experiments. The stimulating electrode was placed 150–200 μm rostral to the recording electrode. The intensity inducing the 60% of the maximum amplitude of EPSC was adopted as the test stimulation, except for the experiment for conducting the input-output (I-O) relationship of EPSCs. For each cell at each stimulus intensity tested, ~20 consecutive EPSCs were recorded and the peak amplitudes were averaged. A series of interpulses interval times (25, 50, 100, and 200 ms) was adopted in the paired-pulse ratio (PPR) test.

To stimulate specific synaptic inputs into NAc slices, a LED illumination (LAMBDA HPX-5, Sutter Instrument) coupled with a band pass excitation filter (470/40 nm) was used in the experiment. Optical stimulation pulse (2 ms, 2–5 mW) was chosen for each cell recording. The $GABA_A$ receptor antagonist PTX (100 μM) was present in the aCSF throughout the experiment. The interpulses interval time containing 50, 100, 200 ms, and 10 s was used in light stimulation evoked PPR test. The AMPAR/NMDAR ratio was calculated by EPSCs (~20 consecutive traces) recorded at −70 mV and then holding the cell to +40 mV and collecting another EPSCs (~20 consecutive traces). The averaged EPSCs peak at −70 mV was measured as the AMPAR-mediated EPSC. The NMDAR-mediated EPSCs were calculated by measuring the value of the averaged EPSCs (held at +40 mV) after 50–55 ms of light stimulation.

Histology and imaging

Animals were deeply anesthetized with isoflurane and perfused intracardially with cold PBS followed by 4% paraformaldehyde (PFA). Brains were removed and postfixed in 4% PFA for 6–8 h at 4°C, and then transferred to PBS. Slices were coronal cut in a cryostat at 30 μm or in a vibratome at 100 μm (Leica VT-1000; Fig. 6*B*). Then slices were washed and mounted. Images were captured using a Nikon fluorescence microscope (Nikon Ni-E) with a 10× objective or confocal microscope (Leica SP8).

Experimental design and statistical analysis

All sample sizes and experimental design were based on previously published data from our lab and similar experiments in the field. All results were presented as the mean ± SEM. Data normality were assessed by the Kolmogorov–Smirnov (K-S) test. Unpaired Student's *t* test was used when datasets passed the normality test. The Mann–Whitney nonparametric test was used for datasets not passing a normal distribution. The number of spikes and the behavioral effect of chemogenetic regulation were analyzed using a two-way repeated measure ANOVA or mixed-effects model. Data were analyzed and graphed using Prism 8.0 software (GraphPad). The criterion for statistical significance was $p < 0.05$.

Results

Intradermal injection of C48/80 decreases the intrinsic excitability of Drd1-MSNs in the NAc core

Intradermal injection of C48/80 is a well-validated histamine-dependent itch model. As previously reported (Sanders et al., 2019), injection of C48/80 caused robust scratching behaviors (Fig. 1*A*). In addition, C48/80-treated mice show less time spent in the open arms and less number of entries into the open arms on the EPM (Fig. 1*B*,*C*). The time spent in the central zone and

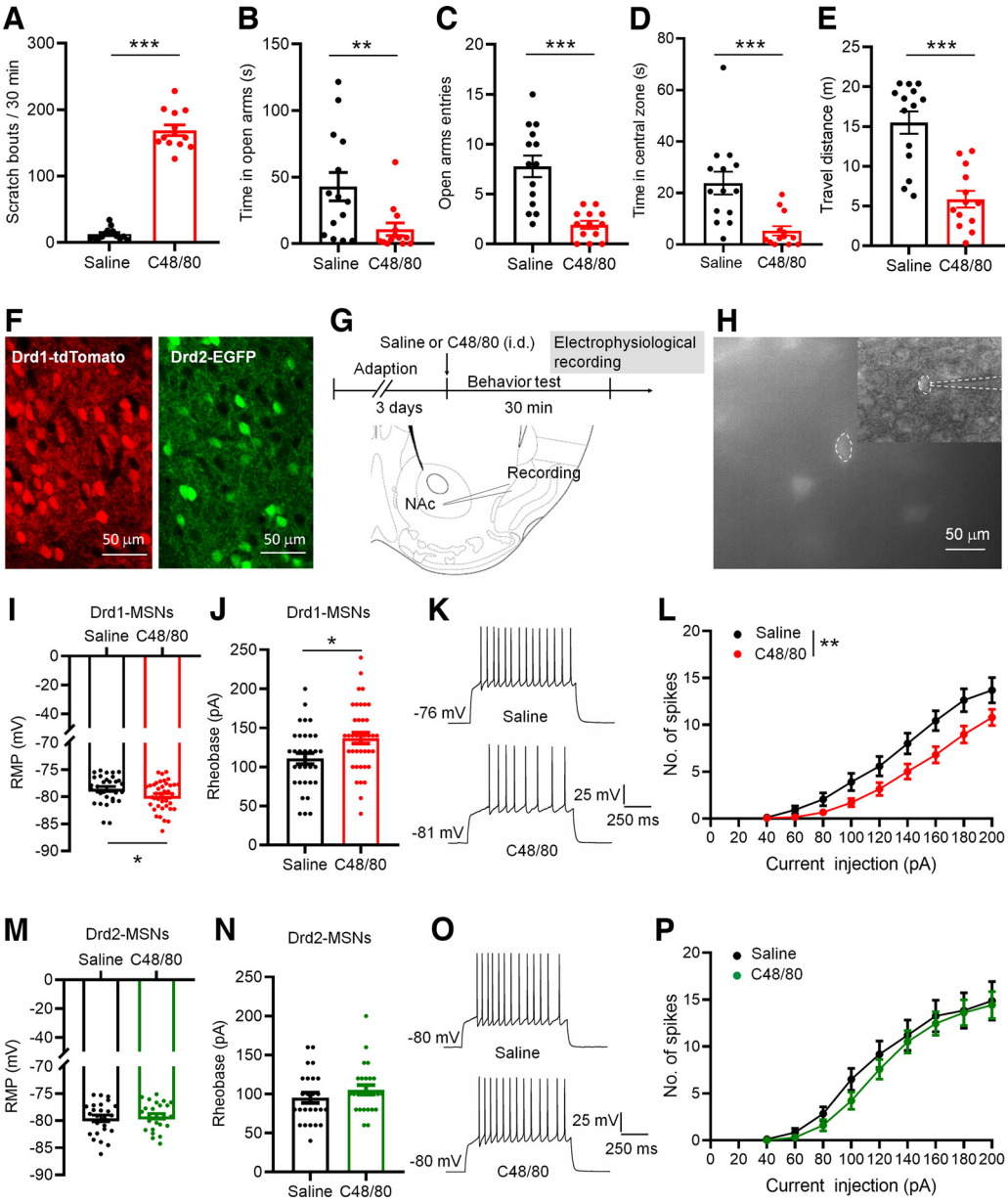

Figure 1. C48/80 reduces intrinsic excitability of Drd1-MSNs in the NAc core. ***A***, Intradermal injection of C48/80 induces scratching bouts in mice ($n = 13$–14 mice/group, $^{***}p < 0.0001$, $U = 0$, Mann–Whitney U test). ***B***, The EPMT shows that C48/80 treatment reduces the time spent in open arms compared with saline injection ($n = 13$–14 mice/group, $^{**}p = 0.0069$, $U = 36.50$, Mann–Whitney U test). ***C***, C48/80 reduces the open arms entries on the EPM ($^{***}p < 0.0001$, $t_{(25)} = 4.94$, Student's t test). ***D***, The OFT shows that C48/80 treatment reduces the time spent in central zone compared with saline injection ($n = 13$–14 mice/group, $^{***}p = 0.0003$; $U = 20$, Mann–Whitney U test). ***E***, C48/80 treatment reduces the travel distance on the OFT ($^{***}p < 0.0001$, $U = 15$, Mann–Whitney U test). ***F***, Representative images show the identification of Drd1-MSNs (left) and Drd2-MSNs (right) in coronal NAc slices from Drd1-tdTomato and Drd2-eGFP mice, respectively. ***G***, Schematic representation of the experimental schedule and recording site. ***H***, A fluorescent-positive neuron was recorded by patch clamp pipette in fluorescent and DIC image modes. ***I***, Bar graph and scatter plot for rest membrane potential (RMP) in Drd1-MSNs in slices from the saline-treated and C48/80-treated mice ($n = 32$–39 neurons/group, $^{*}p = 0.04$ $U = 446.5$, Mann–Whitney U test). ***J***, Same as I for rheobase ($n = 32$–39 neurons/group, $^{*}p = 0.0105$, $t_{(69)} = 2.631$, Student's t test). ***K***, Sample traces of action potentials (APs) obtained in Drd1-MSNs in slices from saline-treated and C48/80-treated mice. ***L***, The number of evoked action potentials in response to the increasing depolarizing current steps in Drd1-MSNs from saline-treated and C48/80-treated mice ($F_{(\text{interaction } 8,536)} = 2.384$, $p = 0.0157$; $F_{(\text{treatments } 1,67)} = 7.241$, $^{**}p = 0.0090$, two-way ANOVA with repeated measure). ***M***, Bar graph and scatter plot for RMP in Drd2-MSNs in slices from the saline-treated (black) and C48/80-treated (green) mice ($n = 25$–26 neurons/group, $p = 0.6261$, $t_{(49)} = 0.4903$, Student's t test). ***N***, Same as ***M*** for rheobase ($n = 25$–26 neurons/group, $p = 0.2363$, $U = 263$, Mann–Whitney U test). ***O***, Sample traces of APs obtained in Drd2-MSNs in slices from saline-treated and C48/80-treated mice. ***P***, The number of evoked action potentials in response to the increasing depolarizing current steps in Drd2-MSNs from saline-treated and C48/80-treated mice ($F_{(\text{interaction } 8,384)} = 0.3561$, $p = 0.9428$; $F_{(\text{treatments } 1,48)} = 4575$, $p = 0.5020$, two-way ANOVA with repeated measure).

travel distance on the OF were decreased in mice treated with C48/80 (Fig. 1*D*,*E*), indicating that C48/80 induces anxiety-like behaviors. We then tested whether C48/80 affects the membrane excitability of Drd1-MSNs and Drd2-MSNs in the NAc core of Drd1-tdTomato and Drd2-EGFP transgenic mice using patch-clamp recordings in brain slices (Fig. 1*F*–*H*). The C48/80 injection resulted in a significantly hyperpolarized RMP in Drd1-MSNs (Fig. 1*I*) and an increased rheobase current (the minimal current necessary to elicit firing; Fig. 1*J*). The number of the evoked action potentials recorded from Drd1-MSNs was decreased in C48/80-treated mice (Fig. 1*K*,*L*). In contrast, the RMP, rheobase current, and evoked action potentials in Drd2-MSNs were comparable between saline and C48/80 groups (Fig. 1*M*–*P*).

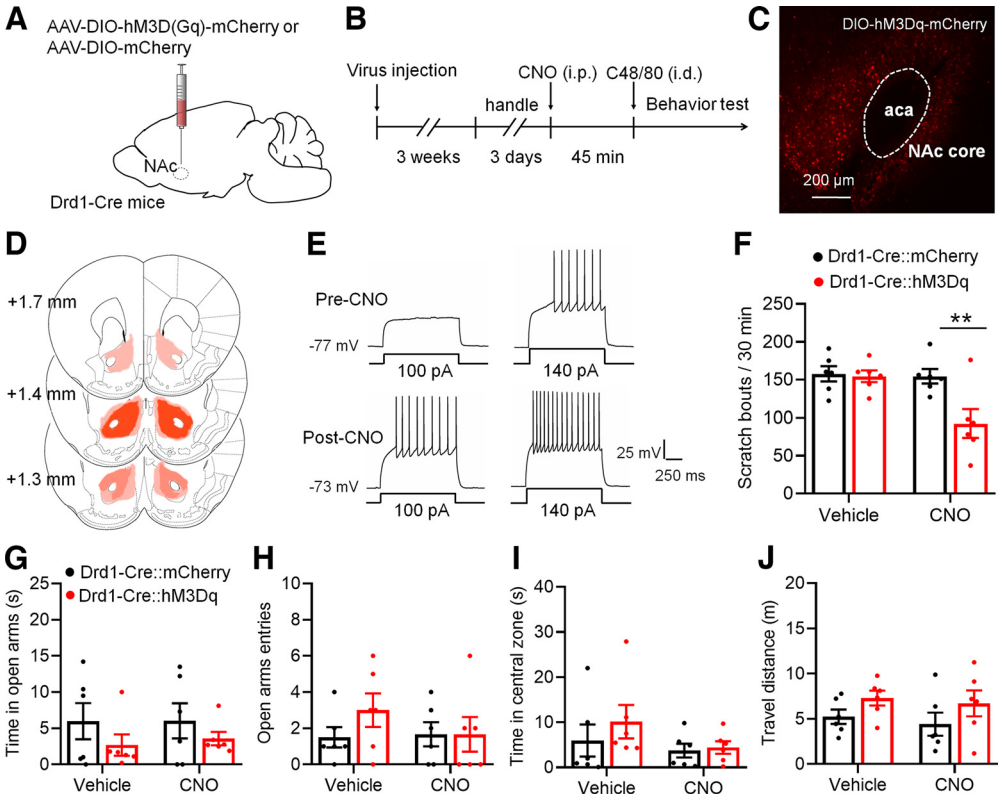

Figure 2. Chemogenetic activation of Drd1-MSNs in the NAc core decreases C48/80-induced scratching behaviors. ***A***, Schematic illustration of virus injection site in the NAc. The AAV-DIO-hM3D(Gq)-mCherry was used for conditional activation of Drd1-MSNs in Drd1-Cre mice. ***B***, Schematic diagram of the time line for the experiment. ***C***, Representative brain section shows the expression of AAV-DIO-hM3Dq-mCherry in the NAc core. aca, anterior commissure, anterior part. ***D***, Viral spread of AAV-DIO-hM3D(Gq)-mCherry and AAV-DIO-mCherry in Drd1-cre mice. Each mouse is represented by one translucent outline, and outlines are overlapped. ***E***, Sample traces shows the injected currents (+100 and +140 pA)-evoked membrane voltage responses recorded in hM3Dq-expressing Drd1-MSNs before and after CNO (5 μM) application. Notably, CNO incubating leads a relatively sustained depolarization on the RMP and increases the firing frequency in hM3Dq-expressing cells. ***F***, Chemogenetic activation of Drd1-MSNs in the NAc core decreases the scratching behaviors in mice treated with C48/80 ($F_{(\text{interaction } 1,10)} = 8.282$, $p = 0.0164$; $F_{(\text{drug } 1,10)} = 10.16$, $p = 0.0097$; $F_{(\text{virus } 1,10)} = 5.298$, $^{**}p = 0.041$). ***G***, The EPMT shows that chemogentic activation of Drd1-MSNs in the NAc core does not change the time spent in open arms in mice treated with C48/80 ($F_{(\text{interaction } 1,10)} = 0.03761$, $p = 0.8501$; $F_{(\text{drug } 1,10)} = 0.04718$, $p = 0.8324$; $F_{(\text{virus } 1,10)} = 2.805$, $p = 0.1249$). ***H***, Same as G for summary of the open arms entry ($F_{(\text{interaction } 1,10)} = 1.462$, $p = 0.2544$; $F_{(\text{drug } 1,10)} = 0.8845$, $p = 0.3691$; $F_{(\text{virus } 1,10)} = 0.6358$, $p = 0.4438$). ***I***, The OFT shows that chemogenetic activation of Drd1-MSNs in the NAc core does not change the time spent in central zone in mice treated with C48/80 ($F_{(\text{interaction } 1,10)} = 0.3991$, $p = 0.5417$; $F_{(\text{drug } 1,10)} = 2.062$, $p = 0.1816$; $F_{(\text{virus } 1,10)} = 0.7666$, $p = 0.4018$). ***J***, Same as I for summary of the travel distance ($F_{(\text{interaction } 1,10)} = 0.01651$, $p = 0.9003$; $F_{(\text{drug } 1,10)} = 0.5096$, $p = 0.4916$; $F_{(\text{virus } 1,10)} = 3.048$, $p = 0.1114$).

Chemogenetic activation of Drd1-MSNs attenuates C48/80-induced scratching behaviors

Based on the alterations of intrinsic excitability in Drd1-MSNs after C48/80, we asked whether the activity of Drd1-MSNs in the NAc core is involved in C48/80-induced scratching and the related anxiety. The AAV-expressing Cre-dependent hM3D(Gq) DREADDs (AAV-DIO-hM3Dq-mCherry) or control AAVs (AAV-DIO-mCherry) were injected into the bilateral NAc core of Drd1-Cre transgenic mice (Fig. 2*A*). Mice were intraperitoneally injected with CNO or vehicle 45 min before the behaviors testing (Fig. 2*B*). The expression of AAVs in the NAc core was confirmed by mCherry fluorescence (Fig. 2*C*,*D*). The *ex vivo* electrophysiological recordings showed that the excitability of Drd1-MSNs infected with AAV-DIO-hM3Dq-mCherry was rapidly increased after CNO perfusion (Fig. 2*E*). The behavioral test showed that CNO significantly suppressed C48/80-induced scratching bouts in mice injected with AAV-DIO-hM3Dq-mCherry (Fig. 2*F*). However, in mice injected with the AAV-DIO-mCherry, CNO did not change the scratching behavior. To test the effect of AAV-DIO-hM3Dq-mCherry in C48/80-induced anxiety-like behavior, the EPMT and OFT were performed. For the EPMT, there was no significant difference in the time spent in the open arms (Fig. 2*G*) and the number of entries into the open arms (Fig. 2*H*) between vehicle and CNO treatment in AAV-DIO-hM3Dq-mCherry-treated or AAV-DIO-mCherry-treated mice. Similarly, the activation of Drd1-MSNs had no effects on the time spent in the central zone (Fig. 2*I*) and travel distance (Fig. 2*J*) on the OFT.

Chemogenetic inhibition of Drd1-MSNs promotes a low dose of C48/80-induced scratching behaviors

We then tested the effect of chemogenetic inhibition of Drd1-MSNs on C48/80-induced behaviors. AAV virus expressing Cre-dependent hM4D(Gi) DREADDs (AAV-DIO-hM4Di-mCherry) or AAV-DIO-mCherry were bilaterally injected in the NAc core in Drd1-Cre transgenic mice. Mice were examined for scratching and anxiety-like behaviors after CNO (or vehicle) and C48/80 injection (Fig. 3*A*,*B*). The virus expression in the NAc core was confirmed by mCherry fluorescence (Fig. 3*C*,*D*). Moreover, the excitability of Drd1-MSNs with AAV-DIO-hM4Di-mCherry infection was markedly decreased after CNO incubation (Fig. 3*E*). However, inhibition of Drd1-MSNs firing by AAV-DIO-hM4Di-mCherry and CNO did not affect C48/80-induced scratching behaviors (Fig. 3*F*). We then checked the effect of the virus on itch induced by a lower dose of C48/80 (10 μg/50 μl). The results showed that inhibition of Drd1-MSNs significantly increased scratching bouts in mice who received the

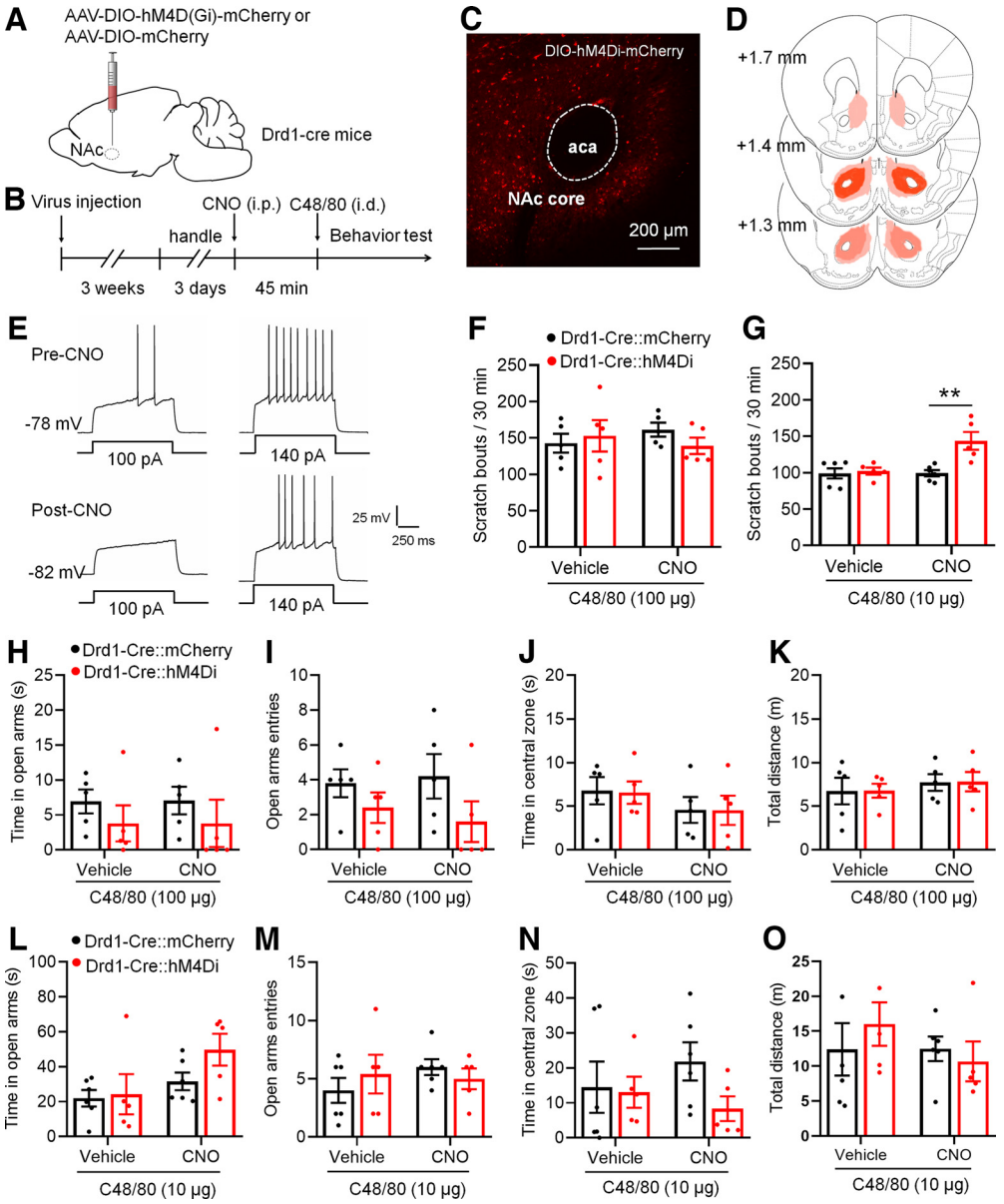

Figure 3. Chemogenetic inhibition of Drd1-MSNs in the NAc core increases C48/80-induced scratching behaviors. ***A***, Schematic illustration of virus injection site in the NAc. The AAV-DIO-hM4Di-mCherry was used for conditional suppression of Drd1-MSNs in Drd1-Cre mice. ***B***, Schematic diagram of the timeline for the experiment. ***C***, Representative brain section shows the expression of AAV-DIO-hM4Di-mCherry in the NAc core. aca, anterior commissure, anterior part. ***D***, Viral spread of AAV-DIO-hM4D(Gi)-mCherry and AAV-DIO-mCherry in Drd1-cre mice. ***E***, Sample traces show the injected currents (+100 and +140 pA)-evoked membrane voltage responses recorded in hM4Di-expressing Drd1-MSNs before and after CNO (5 μM) application. ***F***, Chemogenetic inhibition of Drd1-MSNs in the NAc core does not change the scratching behaviors in mice treated with C48/80 at the dose of 100 μg/50 μl ($F_{(\text{interaction } 1,8)} = 1.099$, $p = 0.3251$; $F_{(\text{drug } 1,8)} = 0.02412$, $p = 0.8804$; $F_{(\text{virus } 1,8)} = 0.1931$, $p = 0.6719$). ***G***, Chemogentic inhibition of Drd1-MSNs in the NAc core enhances the scratching behaviors in mice treated with a lower dose of C48/80 (10 μg/50 μl; $F_{(\text{interaction } 1,9)} = 8.069$, $p = 0.0194$; $F_{(\text{drug } 1,9)} = 8.331$, $p = 0.0180$; $F_{(\text{virus } 1,9)} = 9.858$, $^{**}p = 0.0119$). ***H***, The EMPT shows that inhibition of Drd1-MSNs in the NAc core does not change the time spent in open arms in mice treated with C48/80 (100 μg; $F_{(\text{interaction } 1,8)} = 0.00156$, $p = 0.9695$; $F_{(\text{drug } 1,8)} = 0.00156$, $p = 0.09695$; $F_{(\text{virus } 1,8)} = 1.003$, $p = 0.3459$). ***I***, Same as ***H*** for the summary of the open arms entry ($F_{(\text{interaction } 1,8)} = 0.6857$; $p = 0.4316$, $F_{(\text{drug } 1,8)} = 0.07619$, $p = 0.7895$; $F_{(\text{virus } 1,8)} = 2.388$, $p = 0.1608$). ***J***, The OFT shows that inhibition of Drd1-MSNs in the NAc core does not change the time spent in central zone in mice treated with C48/80 (100 μg; $F_{(\text{interaction } 1,8)} = 0.00249$, $p = 0.9614$; $F_{(\text{drug } 1,8)} = 1.368$, $p = 0.2757$; $F_{(\text{virus } 1,8)} = 0.01299$, $p = 0.9121$). ***K***, Same as ***J*** for summary of the travel distance ($F_{(\text{interaction } 1,8)} = 0.00036$, $p = 0.9852$; $F_{(\text{drug } 1,8)} = 0.4664$, $p = 0.5139$; $F_{(\text{virus } 1,8)} = 0.0117$, $p = 0.9165$). ***L***, Same as ***H*** for results obtained from mice with a lower dose of C48/80 (10 μg) treatment ($F_{(\text{interaction } 1,9)} = 0.6834$, $p = 0.4298$; $F_{(\text{drug } 1,9)} = 3.33$, $p = 0.1013$; $F_{(\text{virus } 1,9)} = 4.310$, $p = 0.0677$). ***M***, Same as ***I*** for the open arms entry ($F_{(\text{interaction } 1,9)} = 0.9605$, $p = 0.3527$; $F_{(\text{drug } 1,9)} = 0.4269$, $p = 0.5299$; $F_{(\text{virus } 1,9)} = 0.04306$, $p = 0.8402$). ***N***, Same as ***J*** for results obtained from mice with a lower dose of C48/80 treatment ($F_{(\text{interaction } 1,9)} = 1.951$, $p = 0.1959$; $F_{(\text{drug } 1,9)} = 0.09541$, $p = 0.7644$; $F_{(\text{virus } 1,9)} = 1.235$, $p = 0.2952$). ***O***, Same as ***K*** for the travel distance ($F_{(\text{interaction } 1,9)} = 1.191$, $p = 0.3035$; $F_{(\text{drug } 1,9)} = 1.129$, $p = 0.3156$; $F_{(\text{virus } 1,9)} = 0.07106$, $p = 0.7958$).

lower dose of C48/80 (Fig. 3*G*). Again, inhibition of Drd1-MSNs had no effect on time spent and entries in the open arms on the EPM or the time spent in the central zone and total travel distance on the OF after either common dose (Fig. 3*H–K*) or lower dose (Fig. 3*L–O*) of C48/80 injection.

Excitatory synaptic input is increased in Drd1-MSNs from C48/80-treated mice

To examine whether the change of neuronal excitability corresponds to the modulation of excitatory synaptic inputs under itch conditions, we measured the excitatory synaptic input to

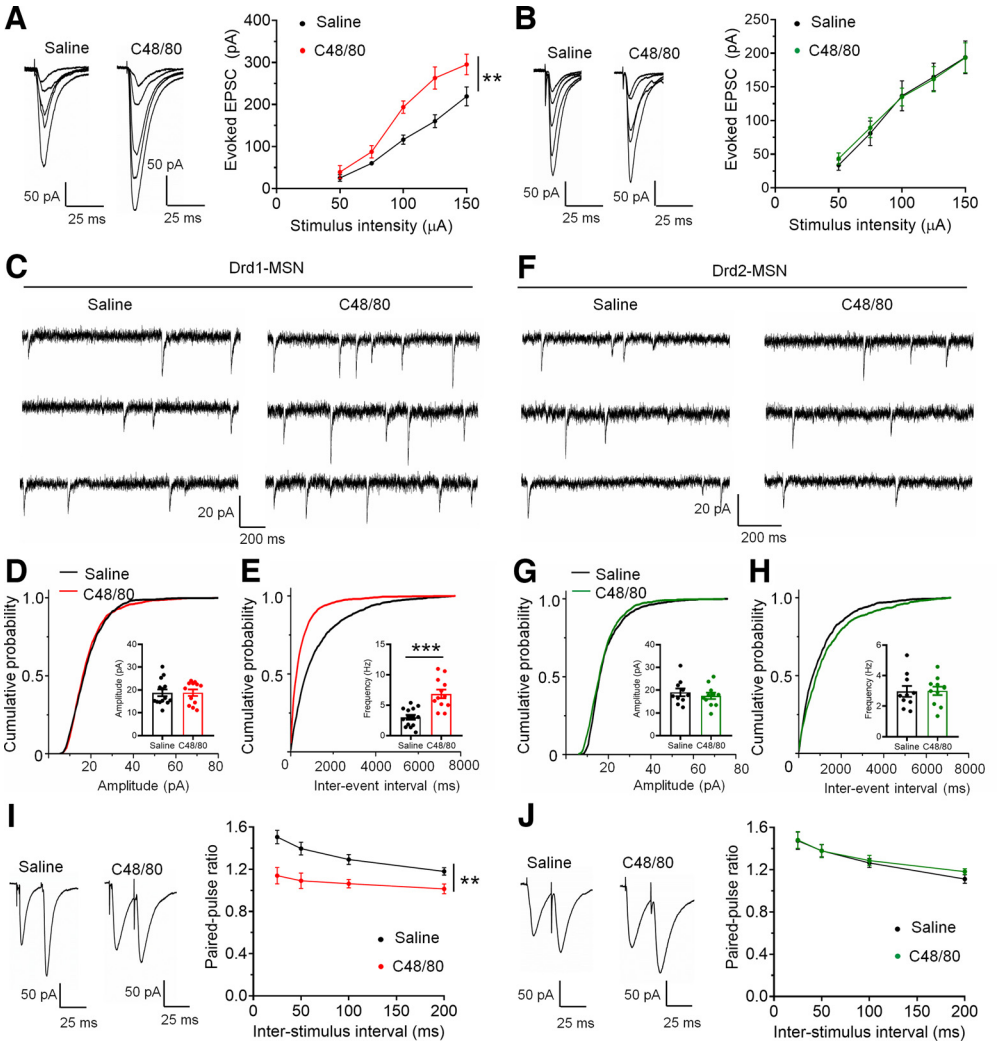

Figure 4. C48/80 increases the efficacy of excitatory transmission onto Drd1-MSNs. ***A***, Averaged traces and summary graph of electrical stimuli-evoked EPSCs for Drd1-MSNs from saline-treated and C48/80-treated mice in response to different stimulus intensity ($n = 6$ neurons/group, $F_{(\text{interaction } 4,40)} = 3.523$, $p = 0.0148$; $F_{(\text{treatments } 1,10)} = 14.66$, $^{**}p = 0.0045$, two-way ANOVA with repeated measure). ***B***, Averaged traces and summary graph of electrical stimuli-evoked EPSCs for Drd2-MSNs from saline-treated and C48/80-treated mice in response to different stimulus intensity ($n = 5$–7 neurons/group, $F_{(\text{interaction } 4,40)} = 0.2464$, $p = 0.9102$; $F_{(\text{treatments } 1,10)} = 0.01156$, $p = 0.9165$, two-way ANOVA with repeated measure). ***C***, Representative traces of sEPSCs obtained in Drd1-MSNs of the NAc core from saline-treated and C48/80-treated mice. ***D***, Cumulative probability of sEPSC event amplitude (K-S test, $p = 0.284$) for a representative Drd1-MSN. Inset, Summary bar graph and scatter plot for sEPSC amplitude in the saline-treated and C48/80-treated mice ($n = 12$–14 neurons/group, $p = 0.8995$, $U = 81$, Mann–Whitney U test). ***E***, Same as ***D*** for cumulative probability of interval between sEPSC events (K-S test, $p < 0.0001$) and sEPSC frequency ($n = 12$–14 neurons/group, $^{***}p < 0.0001$, $t_{(24)} = 4.858$, Student's t test). ***F***, Sample traces of sEPSCs obtained in Drd2-MSNs. ***G***, Cumulative probability of sEPSC event amplitude (K-S test, $p > 0.05$) for Drd2-MSNs. Inset, Summary bar graph and scatter plot for sEPSC amplitude in the saline-treated and C48/80-treated mice ($n = 10$–11 neurons/group, $p = 0.4936$, $t_{(19)} = 0.698$, Student's t test). ***H***, Same as ***G*** for cumulative probability of interval between sEPSC events (K-S test, $p > 0.05$) and sEPSC frequency ($n = 10$–11 neurons/group, $p = 0.9273$, $t_{(19)} = 0.09241$, Student's t test). ***I***, Averaged traces and summary graph of PPR for Drd1-MSNs from saline-treated and C48/80-treated mice at different interstimulus intervals ($n = 8$–9 neurons/group, $F_{(\text{interaction } 3,45)} = 3.488$, $p = 0.0232$; $F_{(\text{treatments } 1,15)} = 14.66$, $^{**}p = 0.0016$, two-way ANOVA with repeated measure). ***J***, Averaged traces and summary graph of PPR for Drd2-MSNs from saline-treated and C48/80-treated mice at different interstimulus intervals ($n = 8$–9 neurons/group, $F_{(\text{interaction } 3,45)} = 0.3581$, $p = 0.7835$, $F_{(\text{treatments } 1,15)} = 0.1289$, $p = 0.7246$, two-way ANOVA with repeated measure).

Drd1- and Drd2-MSNs after saline or C48/80 injection. We first tested the I-O relationships of the glutamatergic transmission established by the amplitude of EPSCs versus the electrical stimulation intensity on Drd1- and Drd2-MSNs. Compared with the saline-treated group, C48/80 increased the magnitude of EPSCs that were evoked with the same intensity in Drd1-MSNs (Fig. 4*A*), but not altered in Drd2-MSNs (Fig. 4*B*). Moreover, in Drd1-MSNs from C48/80-treated mice, there is a significant increase in the frequency of sEPSCs, but not in the amplitude (Fig. 4*C*–*E*). However, C48/80 did not change the frequency or amplitude of sEPSCs in Drd2-MSNs (Fig. 4*F*–*H*). To confirm the presynaptic modulation of glutamate release onto MSNs underlying itch conditions, we recorded electrical stimulation-evoked PPR on Drd1- and Drd2-MSNs. Compared with the saline-treated mice, the PPR of electrical stimulus-evoked EPSCs was substantially decreased in Drd1-MSNs from C48/80-treated mice (Fig. 4*I*). In contrast, C48/80-treated mice displayed no difference from saline-treated mice in the PPR of evoked EPSCs recorded from Drd2-MSNs (Fig. 4*J*). As it was reported that some line of Drd2-EGFP mice are hyperactive (Kramer et al., 2011), we compared the locomotion activity of Drd2-EGFP mice with C57Bl/6 mice. It showed that the travel distance is comparable between the two groups (Drd2-EGFP vs C57Bl/6, 15.5 ± 1.4 vs 16.3 ± 1.7 m, $p = 0.5699$, Mann–Whitney test, $n = 8$–14 mice/group), which is in agreement with previously published reports (Chan et al., 2012), indicating that the data from our Drd2-EGFP mice are reliable.

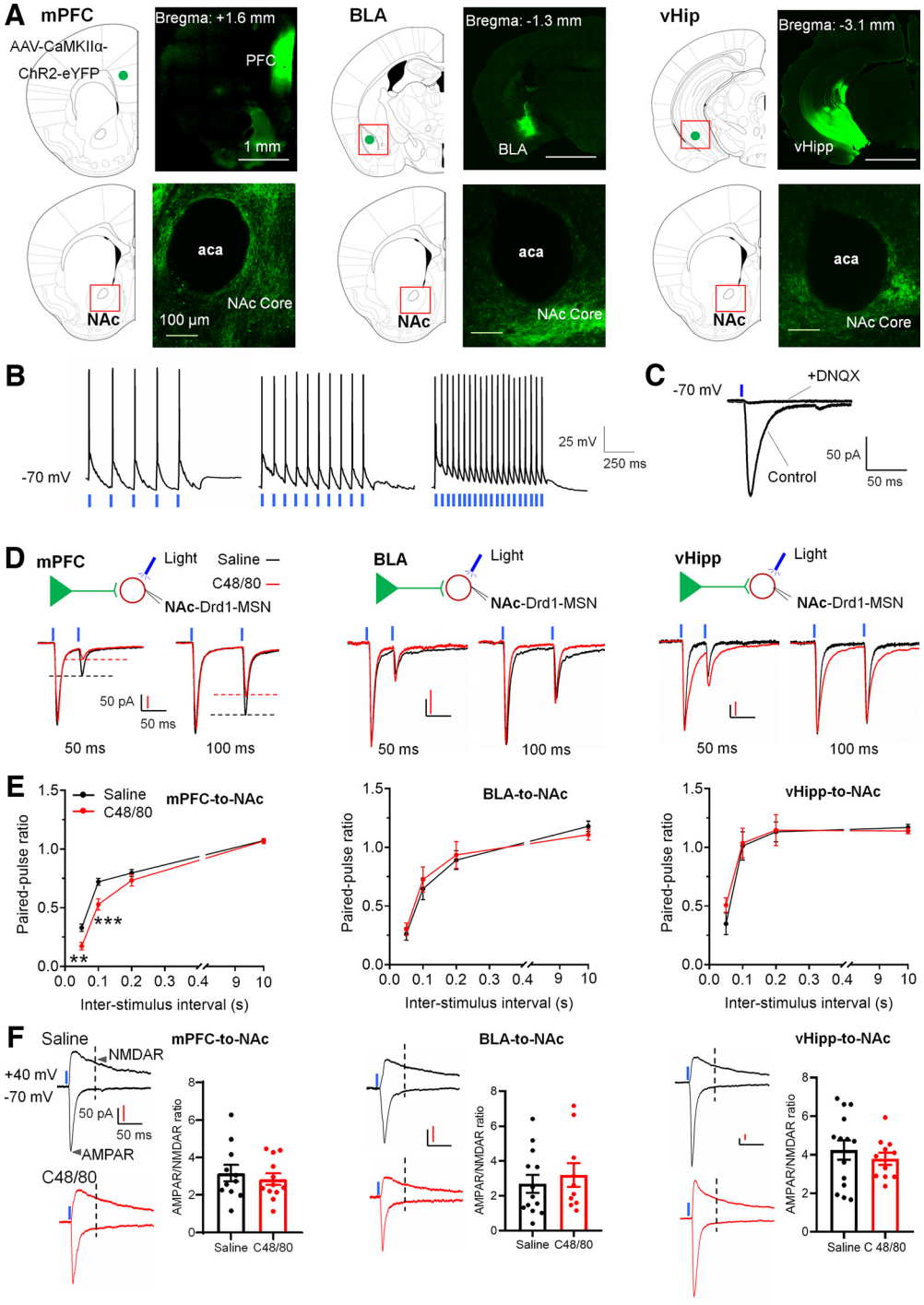

Figure 5. C48/80 increases the projection from the mPFC to Drd1-MSNs in the NAc core. ***A***, Representative coronal brain slices show the expression of AAV-CaMKIIα-ChR2-eYFP in the mPFC, BLA, and vHipp and ChR2-eYFP-containing terminals in the NAc core. aca, anterior commissure, anterior part. ***B***, Representative traces of blue LED light-induced action potentials at different frequencies in ChR2-positive neurons in the mPFC. ***C***, Blue light-induced EPSC recorded from Drd1-MSN at NAc core in the absence or presence of 20 μM of DNQX. ***D***, Sample traces of light-evoked EPSCs for Drd1-MSN in the NAc core obtained from synapses within the mPFC-to-NAc, BLA-to-NAc, or vHipp-to-NAc pathways in saline-treated and C48/80-treated mice. EPSCs recorded at −70 mV with 50- and 100-ms interstimulus intervals. Blue lines show the onset of paired light stimulations. ***E***, Mean PPR values of Drd1-MSNs obtained from synapses within the mPFC-to-NAc ($n = 12$–14 neurons), BLA-to-NAc ($n = 10$–13 neurons), or vHipp-to-NAc ($n = 11$–14 neurons) pathways at different interstimulus intervals in saline-treated and C48/80-treated mice ($F_{(\text{interaction } 3,72)} = 4.872$, $p = 0.0041$; $F_{(\text{treatments } 1,24)} = 10.16$, $p = 0.0040$; two-way ANOVA with repeated measure). $^{**}p < 0.01$; $^{***}p < 0.001$. ***F***, Sample traces of AMPAR-EPSCs and NMDAR-EPSCs (left panel of each group) recorded at −70 and +40 mV on Drd1-MSNs in the NAc core from the light stimulation of different synaptic inputs in saline-treated and C48/80-treated mice. Summary bar graph (right panel of each group) shows the AMPAR/NMDAR response ratios on Drd1-MSNs from the different synaptic inputs in saline-treated and C48/80-treated mice (mPFC input, $n = 11$–12 neurons; BLA input, $n = 10$–13 neurons; vHipp input, $n = 11$–14 neurons).

C48/80 induces pathway-specific changes of glutamatergic synaptic input onto Drd1-MSNs

The NAc receives glutamate synaptic input from the mPFC, BLA, and vHipp (Friedman et al., 2002; Britt et al., 2012). To test which pathway contributes to acute itch-induced presynaptic alterations, we injected AAV-expressing YFP-tagged channel rhodopsin 2 (AAV9-CaMKIIα-ChR2-eYFP) into the mPFC, BLA, or vHipp. Three to four weeks later, notable expression of ChR2 was shown within these regions, and fluorescent axons were concentrated in NAc core (Fig. 5*A*). Then we validated the ChR2 function

in YFP-positive pyramidal neurons in the mPFC and the afferents onto Drd1-MSNs in the NAc. The light-stimulation (470 nm, 2–5 mW, with 5, 10, and 20 Hz for 1 s) evoked stable firing in pyramidal neurons in the mPFC (Fig. 5*B*). Moreover, the light-stimulation-evoked EPSCs in Drd1-MSNs were blocked by adding DNQX (20 μM), an antagonist of AMPA/kainate receptor (Fig. 5*C*). Then we tested the presynaptic efficacies at afferents from mPFC, BLA, or vHipp onto Drd1-MSN in individual groups of animals using PPR. In Drd1-MSNs of the NAc core from C48/80-treated animals, the PPR of light-evoked EPSC at mPFC afferent synapses was significantly decreased, but no change of PPR in BLA- or vHipp-NAc synaptic afferents (Fig. 5*D*,*E*). To clarify whether C48/80 changes the postsynaptic glutamate receptor's function at these afferents onto Drd1-MSNs, we measured the light-evoked currents mediated by AMPA and NMDA receptors. However, there was no difference in AMPAR/NMDAR response ratios in mPFC-, BLA-, or vHipp-NAc synapses between saline and C48/80 injection groups (Fig. 5*F*). These results suggest that C48/80 induces a presynaptic adaptive change in mPFC-NAc projections onto Drd1-MSNs in the NAc core.

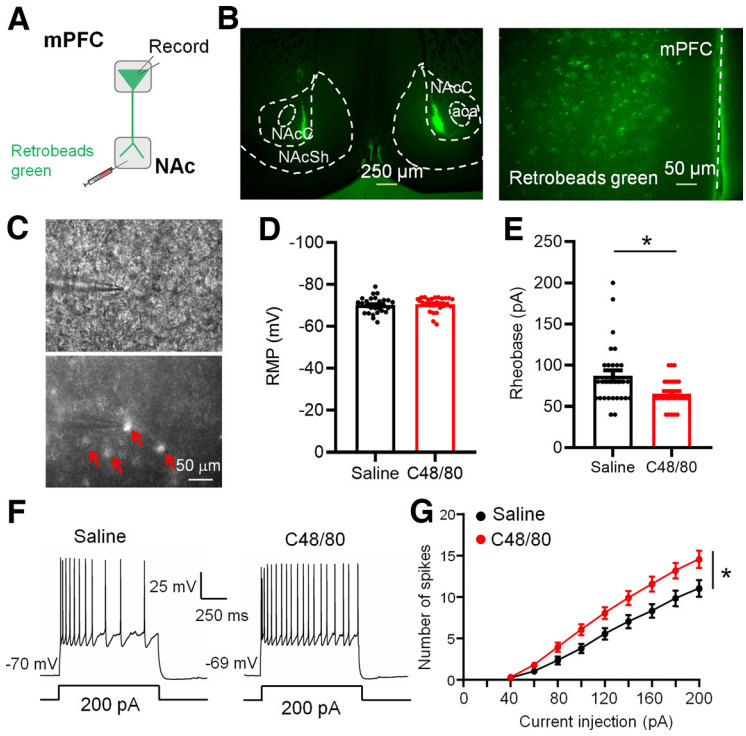

Figure 6. C48/80 increases the excitability of mPFC-to-NAc projection pyramidal neurons. ***A***, Schematic diagram for retrobeads green injection and patch-clamp recording in brain slices. ***B***, Representative coronal brain slices show retrobeads injection sites in the NAc core and retrobeads green-positive neurons (green) in the mPFC. aca, anterior commissure, anterior part; NAcC, NAc core; NAcSh, NAc shell. ***C***, Images show the electrophysiological recording on retrobeads-labeled pyramidal neurons in the mPFC. Red arrows marked the retrobeads-positive neurons. ***D***, Summary bar graph and scatter plot for RMP of green retrobeads-positive PFC-projecting to NAc pyramidal neurons ($n = 27$–29 neurons, $p = 0.3098$, $U = 329$, Mann–Whitney U test). ***E***, Same as ***D*** for rheobase of pyramidal neurons ($n = 27$–29 neurons, $^*p = 0.0110$, $U = 244$, Mann–Whitney U test). ***F***, Sample traces of membrane voltage responses recorded from green retrobeads-positive PFC-projecting to NAc pyramidal neurons from saline-treated or C48/80-treated mice. ***G***, Summarized data show the number of evoked spikes in the groups as indicated in ***F*** ($n = 27$–29 neurons, $F_{(\text{interaction } 8,400)} = 4.816$, $p < 0.0001$; $F_{(\text{treatments } 1,50)} = 6.576$, $^*p = 0.0134$, two-way ANOVA with repeated measure).

The intrinsic excitability of mPFC-NAc projecting neurons is increased in C48/80-injected mice

To test whether C48/80-induced change of transmitter release corresponds to the activity of the upstream region mPFC, the membrane excitability of mPFC-NAc projecting pyramidal neurons was assessed in mice with NAc injection of retrobeads (Fig. 6*A*). Seven days after NAc injection, the retrobeads-positive pyramidal neurons were observed in the mPFC (Fig. 6*B*). We recorded the membrane physiological properties on labeled mPFC-NAc projecting pyramidal neurons in layer V of the PFC slice (Fig. 6*C*). C48/80 did not change the RMP in the mPFC-NAc projecting neurons (Fig. 6*D*), while significantly decreased rheobase currents (Fig. 6*E*). Additionally, the current-induced neuronal firing in mPFC-NAc projecting neurons was significantly increased in C48/80-injected mice (Fig. 6*F*,*G*).

Chemogenetic suppression of mPFC-NAc excitatory synaptic afferents relieves C48/80-induced itch behavior

We then measured whether the changes in the activity of mPFC-NAc excitatory synaptic input are related to itching behaviors. To examine this, AAV virus encoding inhibitory hM4D(Gi) DREADDs (AAV-CaMKIIα-hM4Di-mCherry) or AAV-CaMKIIα-mCherry were bilaterally injected into the mPFC with bilateral implantation the guided cannulas into the NAc core (Fig. 7*A*). Mice were examined for scratching and anxiety-like behaviors after intradermal injection of C48/80 and intra-NAc local infusion of either vehicle or CNO before testing (Fig. 7*B*). The AAV injection site in the mPFC and the axon terminal expression in the NAc core were verified by mCherry fluorescence (Fig. 7*C*,*D*). The behavioral results showed that the CNO infusion into the NAc core significantly suppressed the scratching bouts in mice expressing the AAV-CaMKIIα-hM4Di-mCherry but not in mice expressing AAV-CaMKIIα-mCherry after C48/80 injection (Fig. 7*E*). Furthermore, chemogenetic inhibition of mPFC-NAc core synaptic pathway had no effect on the time spent in the open arms (Fig. 7*F*) and number of entries into the open arms (Fig. 7*G*) on the EPM or the time spent in central zone (Fig. 7*H*) and travel distance (Fig. 7*I*) on the OF.

Pharmacological regulation of KOR in the NAc alters C48/80-induced scratching behaviors

Activation of KOR has been adopted to treat intractable itch (Wikström et al., 2005; Munanairi et al., 2018). Moreover, human functional magnetic resonance imaging showed that the NAc mediates the antipruritic effect of KOR activation (Papoiu et al., 2015). To examine the role of KOR in itch processing, the bilateral guide cannulas were implanted into the NAc core. After the surgery recovery, KOR agonist U50488 was infused into the NAc core and the behaviors were tested (Fig. 8*A*,*B*). U50488 significantly decreased the scratching behavior induced by C48/80 (Fig. 8*C*). There were no effect on the time spent (Fig. 8*D*) and entries (Fig. 8*E*) in the open arms on the EPM, or the time spent in the central zone (Fig. 8*F*) and total travel distance (Fig. 8*G*) on the OF after activation of KOR. In contrast, low dose of C48/80-induced scratching behaviors were significantly increased after the infusion of a KOR antagonist nor-NBI into the NAc core (Fig. 8*H*). On the EPM, there was no significant difference between vehicle-treated and nor-NBI-treated mice in time spent

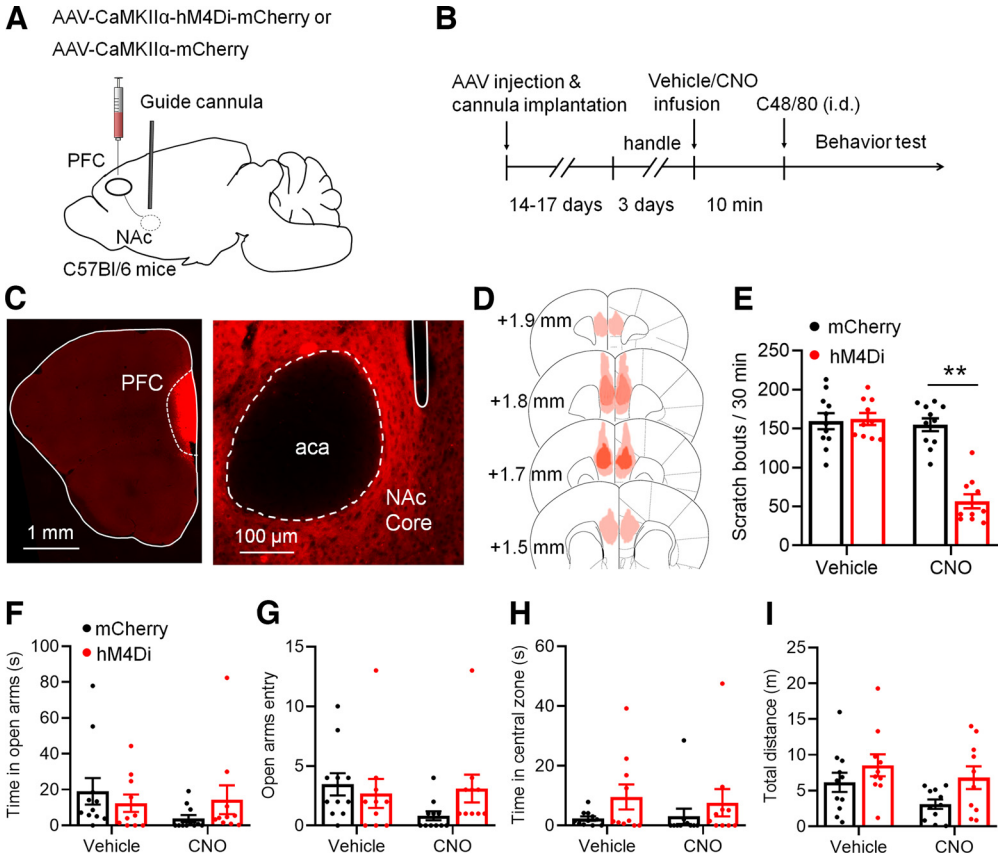

Figure 7. Chemogenetic suppression of glutamatergic synaptic afferents from the mPFC to the NAc core improves C48/80-induced scratching. ***A***, Schematic illustration of virus injection and the guide cannula implantation. ***B***, Schematic diagram of the time line for the experiment. ***C***, Representative brain section shows the expression of hM4Di-mCherry in the PFC and hM4Di-mCherry-containing terminals in the NAc core. aca, anterior commissure, anterior part. ***D***, Viral spread of AAV-CamKIIα-hM4D1-mCherry and AAV-CaMKIIα-mCherry in C57Bl/6 mice. ***E***, Summary bar graph shows that local microinjections of CNO (1 μM) into the NAc core reduces scratching behaviors evoked by C48/80 ($n = 10$–11 mice, $F_{(\text{interaction } 1,19)} = 36.98$, $p < 0.0001$; $F_{(\text{drug } 1,19)} = 43.78$, $p < 0.001$; $F_{(\text{virus } 1,19)} = 25.08$, ***$p < 0.001$). ***F***, The EPMT shows that inhibition of PFC glutamatergic terminals in the NAc does not change the time spent in open arms in mice treated with C48/80 ($F_{(\text{interaction } 1,19)} = 2.629$, $p = 0.1214$; $F_{(\text{drug } 1,19)} = 1.576$, $p = 0.2246$; $F_{(\text{virus } 1,19)} = 0.08392$, $p = 0.7752$). ***G***, Same as ***F*** for summary of the open arms entries ($F_{(\text{interaction } 1,19)} = 2.789$, $p = 0.1113$; $F_{(\text{drug } 1,19)} = 1.513$, $p = 0.2337$; $F_{(\text{virus } 1,19)} = 0.5778$, $p = 0.4565$). ***H***, The OFT shows that inhibition of PFC glutamatergic terminals in the NAc does not change the time spent in central zone in mice treated with C48/80 ($F_{(\text{interaction } 1,19)} = 4342$, $p = 0.5178$; $F_{(\text{drug } 1,19)} = 0.08039$, $p = 0.7798$; $F_{(\text{virus } 1,19)} = 2.023$, $p = 0.1712$). ***I***, Same as ***H*** for summary of the travel distance on the OF ($F_{(\text{interaction } 1,19)} = 0.2559$, $p = 0.6187$; $F_{(\text{drug } 1,19)} = 3.341$, $p = 0.0833$).

in the open arms (Fig. 8*I*) and the number of entries into the open arms (Fig. 8*J*). Similarly, nor-NBI infusion had no effects on the time spent in the central zone (Fig. 8*K*) and travel distance (Fig. 8*L*) on the OF in C48/80-treated animals.

The activity of KOR regulates itch-related synaptic plasticity in the NAc core

To further test the mechanisms underlying KOR-mediated modulation of scratching behavior induced by C48/80, we recorded mEPSCs in the Drd1-MSNs from saline-injected and C48/80-injected mice. We first measured the effects of U50488 on mEPSCs of Drd1-MSNs (Fig. 9*A*). Perfusion of U50488 significantly decreased the frequency of mEPSCs in Drd1-MSN recorded from C48/80-treated animals compared with that in saline-treated mice (Fig. 9*B*). No difference was observed on the amplitude of mESPCs in saline-treated and C48/80-treated mice (Fig. 9*C*). Moreover, inhibition of KOR with nor-NBI increased the frequency of mEPSCs in Drd1-MSNs from C48/80-treated mice (Fig. 9*D*,*E*), with no alterations in the amplitude of mEPSCs (Fig. 9*D*,*F*).

Discussion

Here, we showed that C48/80 decreased the intrinsic membrane excitability in Drd1-MSNs, and chemogenetic activation of Drd1-MSNs attenuated C48/80-induced itch. Moreover, C48/80 increased the excitatory synaptic transmission of Drd1-MSNs from the mPFC, also increased the intrinsic excitability of PFC-NAc projecting pyramidal neurons. Chemogenetic inhibition of the PFC-NAc synaptic pathway relieved C48/80-induced scratching. Furthermore, pharmacological activation of KOR in the NAc suppressed scratching behavior and reduced the presynaptic excitatory inputs to Drd1-MSNs. Our results suggest that Drd1-MSNs and the synaptic inputs from the mPFC play an important role in the regulation of the scratching behaviors induced by itch stimuli, and KOR acts as a negative feedback regulator of Drd1-MSNs at the NAc core under itch conditions.

Neural adaptation of Drd1-MSNs in the NAc core in C48/80-elicited acute itch

As a critical part of the reward circuit, the NAc MSNs receive dopaminergic innervation from the VTA (Stuber et al., 2011). Meanwhile, NAc sends long-range GABAergic synaptic axonal projections to the VTA (Watabe-Uchida et al., 2012; Yang et al., 2018), and these inhibitory inputs play a major role in controlling the activity of DA neurons (Henny et al., 2012). C48/80 decreased the intrinsic excitability of Drd1-MSNs in the NAc, which may reduce the inhibition on VTA DA neurons and increase the release of DA to the NAc. Indeed, the activity of

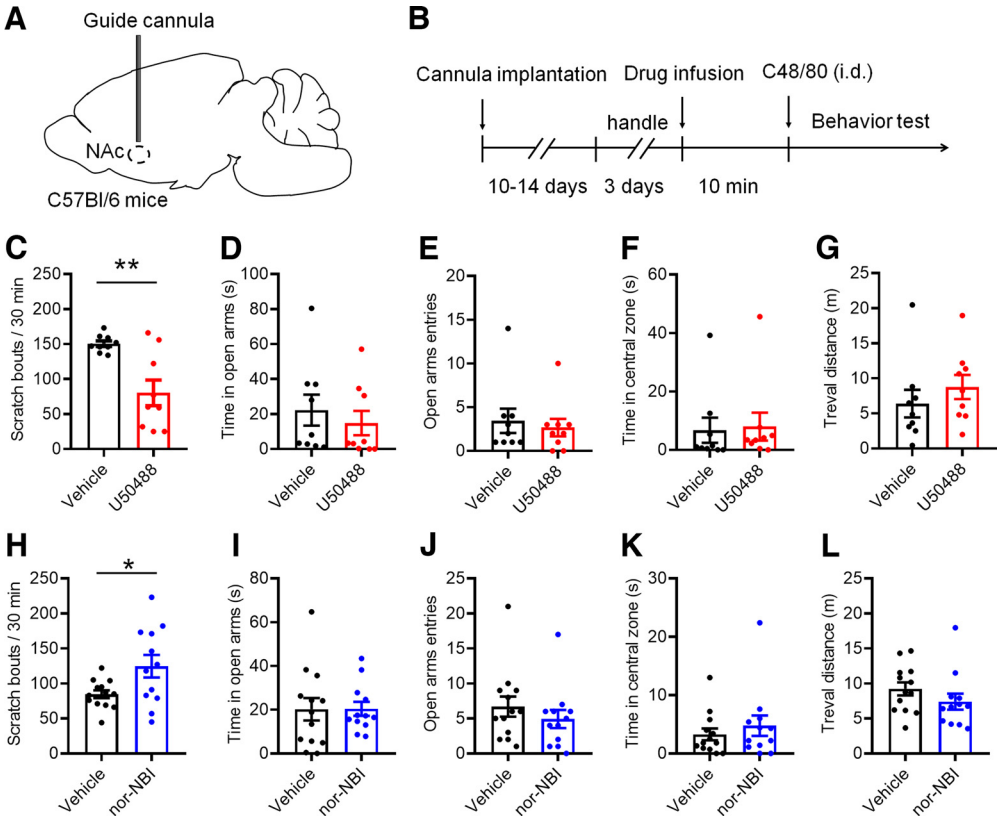

Figure 8. Regulation of KOR in the NAc alters C48/80-induced scratching behaviors. ***A***, Experimental configuration shows guide cannula implantation in the NAc core. ***B***, Schematic diagram of the timeline for the experiment. ***C***, Bilateral intra-NAc core infusion of KOR agonist U50488 (0.26 μg/0.3 μl per side) significantly attenuates C48/80-induced scratching behaviors ($n = 9$ mice for each group, $t_{(16)} = 3.749$, $^{**}p = 0.0018$). ***D***, NAc administration of U50488 does not affect the time spent in open arms in mice with treated with C48/80 ($U = 30.50$, $p = 0.3980$). ***E***, Same as ***D*** for the open arms entry ($U = 35.50$, $p = 0.6853$). ***F***, U50488 does not affect the time spent in central zone in mice with treated with C48/80 ($U = 31.50$, $p = 0.4489$). ***G***, Same as ***F*** for the travel distance ($U = 28$, $p = 0.2973$). ***H***, Intra-NAc core preinfusion of KOR antagonist nor-NBI (0.25 μg/0.3 μl per side) increases the low-dose (10 μg/50 μl) of C48/80-induced scratching behaviors ($n = 12$–13 mice for each group, $t_{(23)} = 2.429$, $^{*}p = 0.0234$). ***I***, nor-NBI did not affect the time spent in open arms in mice treated with C48/80 (10 μg; $t_{(23)} = 0.03014$, $p = 0.9762$). ***J***, Same as I for the open arms entry ($U = 57$, $p = 0.2611$). ***K***, nor-NBI did not affect the time spent in central zone in mice treated with C48/80 ($U = 65$, $p = 0.4936$). ***L***, Same as ***K*** for the travel distance ($U = 51$, $p = 0.1519$).

VTA DA neurons was increased during scratching behavior (Yuan et al., 2018; Su et al., 2019), and repeated activation of dopamine receptors on NAc neurons caused a reduction of membrane excitability (O'Donnell and Grace, 1996). Meanwhile, Drd1-MSNs suppress the tonic activity of VTA GABA neurons (Bocklisch et al., 2013), and the decreased intrinsic excitability of Drd1-MSNs may also contribute to the increased activity of GABA neurons under acute itch conditions, which mediates itch-related aversion (Su et al., 2019). Our data also showed that the RMP was hyperpolarized in Drd1-MSNs, which may also contribute to the decreased neuronal excitability after itch stimuli. However, the intrinsic excitability of Drd2-MSNs was not changed after C48/80 injection, indicating a different role of these two subtypes in mediating itch.

The Drd1-MSNs play a crucial role in regulating the desire and motivation in reward-related behaviors (Calipari et al., 2016). Moreover, activation of NAc Drd1-MSNs results in resilient behavioral outcomes, while inhibition of these MSNs induces depression-like outcomes after chronic social defeat stress (CSDC; Francis et al., 2015). Chemogenetic activation of Drd1-MSNs decreased the scratching behaviors, which may be because of the increased GABAergic inhibition on dopaminergic neurons in the VTA (Yang et al., 2018). Meanwhile, chemogenetic inhibition of Drd1-MSNs enhanced scratching bouts in the low dose of C48/80 exposure but did not in the normal dose of C48/80 injection, which may attribute to the relative ceiling effect of C48/80 on scratching production (Kuraishi et al., 1995). However, chemogenetic regulation of the activity of NAc Drd1-MSNs had no effect on itch-elicited anxiety-like behaviors, suggesting that the motivation to scratch may be separated from the anxiety-like behaviors.

NAc MSNs are a special type of GABAergic inhibitory neurons without spontaneous action potentials discharge, causing its activity depend on synaptic afferents. Itch stimuli increased the frequency but not the amplitude of sEPSCs in Drd1-MSNs, suggesting a presynaptic change in Drd1-MSNs, which was confirmed by measuring the electrical stimuli-evoked EPSC PPR, further suggesting that the adaption of presynaptic mechanism may increase the I-O relationship of EPSCs in Drd1-MSNs under itch conditions. The itch-elicited scratching behavior is highly associated with an increase in NAc DA level (Yuan et al., 2018), and DA or Drd1 agonist increased sEPSC frequency in Drd1-MSNs, while Drd2 agonist decreased sEPSCs frequency in Drd2-MSNs (André et al., 2010). Meanwhile, the excitatory transmission was decreased in NAc Drd2-MSNs in inflammatory pain model (Schwartz et al., 2014). Notably, the increased presynaptic transmission is associated with the decreased membrane excitability of Drd1-MSNs after C48/80 injection, suggesting a synapse-membrane homeostatic regulation under acute itch conditions. An increase in the excitatory synaptic strength causes a homeostatic decrease in the intrinsic membrane excitability of NAc MSNs, which tends to stabilize the functional output of neuron

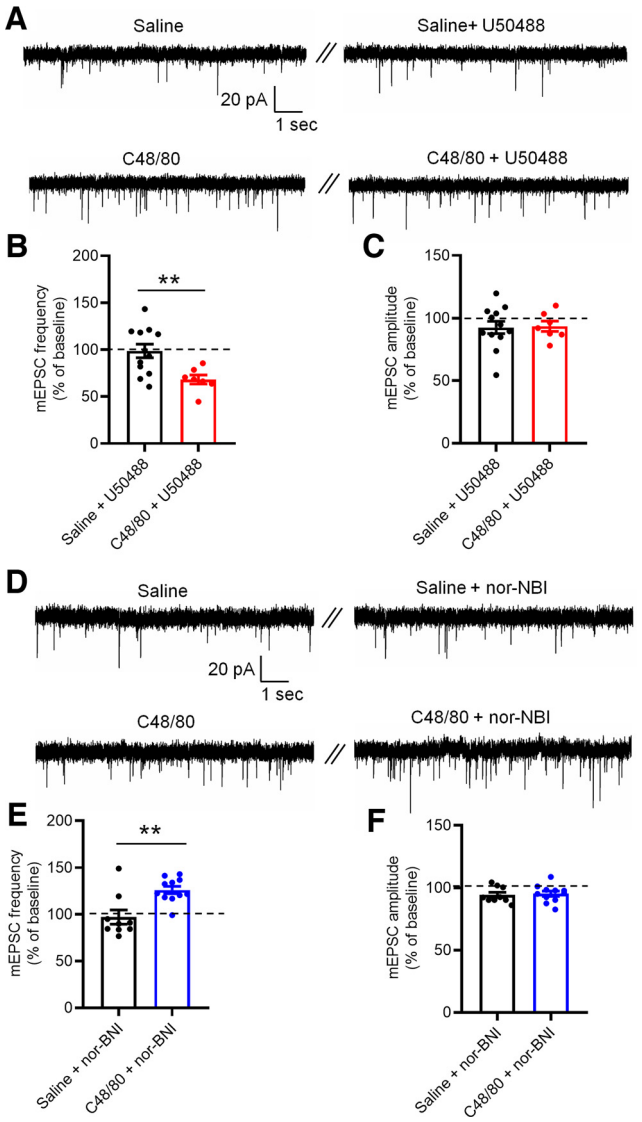

Figure 9. KOR activity changes the frequency of mEPSCs in Drd1-MSNs after C48/80 treatment. ***A***, Sample traces of mEPSCs recorded in Drd1-MSNs at NAc core from saline-treated and C48/80-treated mice before and during application of U50488 (1 μM). ***B***, Summary of the effects of U50488 on the frequency of mEPSCs recorded from saline and C48/80 treated mice ($n = 7$–12 neurons, $t_{(17)} = 2.943$, $^{**}p = 0.0091$). ***C***, Summary of the effects of U50488 on the amplitude of mEPSCs ($t_{(17)} = 0.1314$, $p = 0.8970$). ***D***, Same as A for mEPSCs obtained in the absence or presence of nor-NBI (0.1 μM) from saline-treated and C48/80-treated mice. ***E***, Summary of the effects of nor-NBI on the frequency of mEPSCs recorded from saline-treated and C48/80-treated mice ($n = 9$–11 neurons, $U = 14$, $^{**}p = 0.0057$). ***F***, Summary of the effects of nor-NBI on the amplitude of mEPSC ($t_{(18)} = 0.3375$, $p = 0.7396$).

(Ishikawa et al., 2009; J. Wang et al., 2018). It was reported that the upregulation of glutamate receptor NR2B leads to a decrease in the membrane excitability of NAc MSNs after short-term cocaine withdrawal (J. Wang et al., 2018). The molecular mechanism underlying the decrease of the membrane excitability of Drd1-MSNs after C48/80 needs further investigation.

mPFC-NAc projections are adaptively changed and implicated in itch-related scratching

Glutamatergic synaptic afferents from multiple limbic and paralimbic regions to the NAc MSNs contribute to the regulation of motivation and anxiety (Stuber et al., 2011; Calhoon and Tye, 2015; X.Y. Zhang et al., 2020). C48/80 did not change the AMPAR/NMDAR current ratio from mPFC, vHipp, and BLA, suggesting that the postsynaptic mechanism is not involved in acute itch. Similarly, cocaine exposure selectively increases the presynaptic release probability of the PFC-NAc synapses but does not change the BLA-NAc synapses (Suska et al., 2013). Differently, nerve injury-induced or inflammation-induced chronic pain causes long-term changes in postsynaptic AMPAR and NMDARs, and a decrease in the related motivation (Ren et al., 2016).

Some cortex regions including mPFC, ACC, and insular cortex are activated under itch conditions (Dhand and Aminoff, 2014; Chen and Sun, 2020). C48/80 increased the intrinsic excitability of PFC-NAc projecting pyramidal neurons, which corresponds to the increase of glutamate release at the presynaptic terminals of these projection neurons in the NAc since the frequency of the action potential is closely related to glutamate transmitter release (Kaczmarek and Zhang, 2017). In agreement with the current study, c-fos expression was increased in the mPFC and ACC regions but not in BLA in mice with histamine-induced acute itch (Lu et al., 2018). Chemogenetic inhibition of PFC reduced both histaminergic and nonhistaminergic itch-induced scratching (Li et al., 2021). Here, selective inhibition of the mPFC-NAc projection reduced C48/80-induced scratching behaviors. However, it seems contradictory to the increased scratching after the inhibition of Drd1-MSNs, which may be because of the complicated local circuitry in the NAc. Drd1-MSNs receive not only excitatory inputs from pPFC, vHipp, and BLA and DAergic input from VTA, but also inhibitory inputs from local GABAergic Drd2-MSNs, cholinergic and fast-spiking GABAergic interneurons (Stuber et al., 2012). The inhibition of mPFC-NAc projection or activation of KOR may lead to the changes of other pathways and indirectly regulate the excitability of Drd1-MSNs.

Optogenetic regulation of mPFC or mPFC-NAc axonal terminals changes pain-related negative emotions (Lee et al., 2015; Martinez et al., 2017; Zhou et al., 2018). However, inhibition of the mPFC-NAc pathway did not change itch-related anxiety behaviors. It was reported that selective stimulation of the mPFC-NAc pathway did not change anxiety-like behavior on OFT, but inhibition of the vHipp-NAc pathway improves the depressive emotion in the CSDS model (Bagot et al., 2015), supporting that pathway-specific regulation of excitatory afferent onto the NAc displays disparate behavioral and physiological responses (Stuber et al., 2012). The neural circuits for coding the anxiety-like behaviors in itch require additional experiments.

KOR activation regulates acute itch via a presynaptic mechanism in the NAc core

Human studies showed that injection with butorphanol, a pronounced KOR affinity agonist, suppresses histamine-evoked itch via the activation of NAc and septal nuclei (Papoiu et al., 2015). Systemic activation of KOR prevents the scratching behaviors induced by chloroquine in male mice (Brust et al., 2016). Consistently, we found that activation of KOR in the NAc core attenuated C48/80-elicited scratching. KOR is expressed on presynaptic terminals of glutamate, dopamine, and serotonin inputs to the NAc (Karkhanis et al., 2016; Rose et al., 2016; Fontaine et al., 2022). Dynorphin is known to be the endogenous ligand of KOR, which is predominantly expressed in Drd1-MSNs in the NAc. The decrease of excitability of Drd1-MSNs after C48/80 may cause a reduction of dynorphin release. The activation of KORs inhibited excitatory synaptic transmission on Drd1-MSNs in itch animals, which may

be because of negative feedback inhibition of KOR on the excitatory synaptic inputs from the mPFC (Hjelmstad and Fields, 2001). Glutamatergic afferents into Drd1-MSNs but not into Drd2-MSNs are more sensitive to KOR inhibition, and KOR inhibits BLA-NAc excitatory synaptic transmission in Drd1-MSNs (Tejeda et al., 2017). Moreover, activation of KOR in the caudal NAc shell or rostral NAc shell increased or decreased anxiety-like behaviors, respectively (Pirino et al., 2020). We found that C48/80-induced anxiety-like behaviors were not changed by KOR ligand in the NAc core, indicating that KOR modulates itch-related behaviors potentially via a cell-type and neural circuit-specific manner.

In summary, our study elucidated the role of NAc MSN subtypes and their glutamatergic excitatory afferents in itch-related behaviors. These results demonstrated that the synaptic connections from mPFC to NAc core shaped the itch stimuli-elicited scratching behavior. In addition, NAc KOR acts as a negative feedback regulator to drive itch-elicited scratching. Thus, specific regulation of the projection from mPFC to Drd1-MSNs or regulation of KOR in NAc core may provide effective strategies for the treatment of itch. It is worth noting that the current study was performed in male mice, whether the mechanisms work in female mice need further investigation.

References

André VM, Cepeda C, Cummings DM, Jocoy EL, Fisher YE, William Yang X, Levine MS (2010) Dopamine modulation of excitatory currents in the striatum is dictated by the expression of D1 or D2 receptors and modified by endocannabinoids. Eur J Neurosci 31:14–28.

Bagot RC, Parise EM, Peña CJ, Zhang HX, Maze I, Chaudhury D, Persaud B, Cachope R, Bolaños-Guzmán CA, Cheer JF, Deisseroth K, Han MH, Nestler EJ (2015) Ventral hippocampal afferents to the nucleus accumbens regulate susceptibility to depression. Nat Commun 6:7062.

Bartels DJ, van Laarhoven AI, van de Kerkhof PC, Evers AW (2016) Placebo and nocebo effects on itch: effects, mechanisms, and predictors. Eur J Pain 20:8–13.

Bocklisch C, Pascoli V, Wong JC, House DR, Yvon C, de Roo M, Tan KR, Lüscher C (2013) Cocaine disinhibits dopamine neurons by potentiation of GABA transmission in the ventral tegmental area. Science 341:1521–1525.

Britt JP, Benaliouad F, McDevitt RA, Stuber GD, Wise RA, Bonci A (2012) Synaptic and behavioral profile of multiple glutamatergic inputs to the nucleus accumbens. Neuron 76:790–803.

Brust TF, Morgenweck J, Kim SA, Rose JH, Locke JL, Schmid CL, Zhou L, Stahl EL, Cameron MD, Scarry SM, Aubé J, Jones SR, Martin TJ, Bohn LM (2016) Biased agonists of the kappa opioid receptor suppress pain and itch without causing sedation or dysphoria. Sci Signal 9:ra117.

Calhoon GG, Tye KM (2015) Resolving the neural circuits of anxiety. Nat Neurosci 18:1394–1404.

Calipari ES, Bagot RC, Purushothaman I, Davidson TJ, Yorgason JT, Peña CJ, Walker DM, Pirpinias ST, Guise KG, Ramakrishnan C, Deisseroth K, Nestler EJ (2016) In vivo imaging identifies temporal signature of D1 and D2 medium spiny neurons in cocaine reward. Proc Natl Acad Sci U S A 113:2726–2731.

Chan CS, Peterson JD, Gertler TS, Glajch KE, Quintana RE, Cui Q, Sebel LE, Plotkin JL, Shen W, Heiman M, Heintz N, Greengard P, Surmeier DJ (2012) Strain-specific regulation of striatal phenotype in Drd2-eGFP BAC transgenic mice. J Neurosci 32:9124–9132.

Chartoff EH, Ebner SR, Sparrow A, Potter D, Baker PM, Ragozzino ME, Roitman MF (2016) Relative timing between kappa opioid receptor activation and cocaine determines the impact on reward and dopamine release. Neuropsychopharmacology 41:989–1002.

Chen XJ, Sun YG (2020) Central circuit mechanisms of itch. Nat Commun 11:3052.

Chisholm A, Rizzo D, Fortin E, Moman V, Quteishat N, Romano A, Capolicchio T, Shalev U (2021) Assessing the role of corticothalamic and thalamo-accumbens projections in the augmentation of heroin seeking in chronically food-restricted rats. J Neurosci 41:354–365.

Dhand A, Aminoff MJ (2014) The neurology of itch. Brain 137:313–322.

Floresco SB (2015) The nucleus accumbens: an interface between cognition, emotion, and action. Annu Rev Psychol 66:25–52.

Fontaine HM, Silva PR, Neiswanger C, Tran R, Abraham AD, Land BB, Neumaier JF, Chavkin C (2022) Stress decreases serotonin tone in the nucleus accumbens in male mice to promote aversion and potentiate cocaine preference via decreased stimulation of 5-HT1B receptors. Neuropsychopharmacology 47:891–901.

Francis TC, Chandra R, Friend DM, Finkel E, Dayrit G, Miranda J, Brooks JM, Iñiguez SD, O'Donnell P, Kravitz A, Lobo MK (2015) Nucleus accumbens medium spiny neuron subtypes mediate depression-related outcomes to social defeat stress. Biol Psychiatry 77:212–222.

Friedman DP, Aggleton JP, Saunders RC (2002) Comparison of hippocampal, amygdala, and perirhinal projections to the nucleus accumbens: combined anterograde and retrograde tracing study in the macaque brain. J Comp Neurol 450:345–365.

Henny P, Brown MT, Northrop A, Faunes M, Ungless MA, Magill PJ, Bolam JP (2012) Structural correlates of heterogeneous in vivo activity of midbrain dopaminergic neurons. Nat Neurosci 15:613–619.

Hjelmstad GO, Fields HL (2001) Kappa opioid receptor inhibition of glutamatergic transmission in the nucleus accumbens shell. J Neurophysiol 85:1153–1158.

Ishikawa M, Mu P, Moyer JT, Wolf JA, Quock RM, Davies NM, Hu XT, Schlüter OM, Dong Y (2009) Homeostatic synapse-driven membrane plasticity in nucleus accumbens neurons. J Neurosci 29:5820–5831.

Jing PB, Cao DL, Li SS, Zhu M, Bai XQ, Wu XB, Gao YJ (2018) Chemokine receptor CXCR3 in the spinal cord contributes to chronic itch in mice. Neurosci Bull 34:54–63.

Kaczmarek LK, Zhang Y (2017) Kv3 channels: enablers of rapid firing, neurotransmitter release, and neuronal endurance. Physiol Rev 97:1431–1468.

Kallupi M, Wee S, Edwards S, Whitfield TW Jr, Oleata CS, Luu G, Schmeichel BE, Koob GF, Roberto M (2013) Kappa opioid receptor-mediated dysregulation of gamma-aminobutyric acidergic transmission in the central amygdala in cocaine addiction. Biol Psychiatry 74:520–528.

Karkhanis AN, Rose JH, Weiner JL, Jones SR (2016) Early-life social isolation stress increases kappa opioid receptor responsiveness and downregulates the dopamine system. Neuropsychopharmacology 41:2263–2274.

Kramer PF, Christensen CH, Hazelwood LA, Dobi A, Bock R, Sibley DR, Mateo Y, Alvarez VA (2011) Dopamine D2 receptor overexpression alters behavior and physiology in Drd2-EGFP mice. J Neurosci 31:126–132.

Kreitzer AC (2009) Physiology and pharmacology of striatal neurons. Annu Rev Neurosci 32:127–147.

Kuraishi Y, Nagasawa T, Hayashi K, Satoh M (1995) Scratching behavior induced by pruritogenic but not algesiogenic agents in mice. Eur J Pharmacol 275:229–233.

Lavery MJ, Stull C, Kinney MO, Yosipovitch G (2016) Nocturnal pruritus: the battle for a peaceful night's sleep. Int J Mol Sci 17:425.

Lee M, Manders TR, Eberle SE, Su C, D'Amour J, Yang R, Lin HY, Deisseroth K, Froemke RC, Wang J (2015) Activation of corticostriatal circuitry relieves chronic neuropathic pain. J Neurosci 35:5247–5259.

LeGates TA, Kvarta MD, Tooley JR, Francis TC, Lobo MK, Creed MC, Thompson SM (2018) Reward behaviour is regulated by the strength of hippocampus-nucleus accumbens synapses. Nature 564:258–262.

Li X, Yao J, Hu KH, Wu B, Sui JF, Gao J, Wu GY, Liu SL (2021) Differential roles of prelimbic and anterior cingulate cortical region in the modulation of histaminergic and non-histaminergic itch. Behav Brain Res 411:113388.

Lu YC, Wang YJ, Lu B, Chen M, Zheng P, Liu JG (2018) ACC to dorsal medial striatum inputs modulate histaminergic itch sensation. J Neurosci 38:3823–3839.

Martinez E, Lin HH, Zhou H, Dale J, Liu K, Wang J (2017) Corticostriatal regulation of acute pain. Front Cell Neurosci 11:146.

Massaly N, et al. (2019) Pain-induced negative affect is mediated via recruitment of the nucleus accumbens kappa opioid system. Neuron 102:564–573.e6.

Mochizuki H, Tanaka S, Morita T, Wasaka T, Sadato N, Kakigi R (2014) The cerebral representation of scratching-induced pleasantness. J Neurophysiol 111:488–498.

Mochizuki H, Papoiu ADP, Nattkemper LA, Lin AC, Kraft RA, Coghill RC, Yosipovitch G (2015) Scratching induces overactivity in motor-related

regions and reward system in chronic itch patients. J Invest Dermatol 135:2814–2823.
Mu P, Neumann PA, Panksepp J, Schlüter OM, Dong Y (2011) Exposure to cocaine alters dynorphin-mediated regulation of excitatory synaptic transmission in nucleus accumbens neurons. Biol Psychiatry 69:228–235.
Munanairi A, et al. (2018) Non-canonical opioid signaling inhibits itch transmission in the spinal cord of mice. Cell Rep 23:866–877.
Murota H, Kitaba S, Tani M, Wataya-Kaneda M, Azukizawa H, Tanemura A, Umegaki N, Terao M, Kotobuki Y, Katayama I (2010) Impact of sedative and non-sedative antihistamines on the impaired productivity and quality of life in patients with pruritic skin diseases. Allergol Int 59:345–354.
O'Donnell P, Grace AA (1996) Dopaminergic reduction of excitability in nucleus accumbens neurons recorded in vitro. Neuropsychopharmacology 15:87–97.
Papoiu AD, Nattkemper LA, Sanders KM, Kraft RA, Chan YH, Coghill RC, Yosipovitch G (2013) Brain's reward circuits mediate itch relief. A functional MRI study of active scratching. PLoS One 8:e82389.
Papoiu ADP, Kraft RA, Coghill RC, Yosipovitch G (2015) Butorphanol suppression of histamine itch is mediated by nucleus accumbens and septal nuclei: a pharmacological fMRI study. J Invest Dermatol 135:560–568.
Phan NQ, Lotts T, Antal A, Bernhard JD, Ständer S (2012) Systemic kappa opioid receptor agonists in the treatment of chronic pruritus: a literature review. Acta Derm Venereol 92:555–560.
Pirino BE, Spodnick MB, Gargiulo AT, Curtis GR, Barson JR, Karkhanis AN (2020) Kappa-opioid receptor-dependent changes in dopamine and anxiety-like or approach-avoidance behavior occur differentially across the nucleus accumbens shell rostro-caudal axis. Neuropharmacology 181:108341.
Ren W, Centeno MV, Berger S, Wu Y, Na X, Liu X, Kondapalli J, Apkarian AV, Martina M, Surmeier DJ (2016) The indirect pathway of the nucleus accumbens shell amplifies neuropathic pain. Nat Neurosci 19:220–222.
Rose JH, Karkhanis AN, Chen R, Gioia D, Lopez MF, Becker HC, McCool BA, Jones SR (2016) Supersensitive kappa opioid receptors promotes ethanol withdrawal-related behaviors and reduce dopamine signaling in the nucleus accumbens. Int J Neuropsychopharmacol 19:pyv127.
Samineni VK, Grajales-Reyes JG, Grajales-Reyes GE, Tycksen E, Copits BA, Pedersen C, Ankudey ES, Sackey JN, Sewell SB, Bruchas MR, Gereau RW (2021) Cellular, circuit and transcriptional framework for modulation of itch in the central amygdala. Elife 10:e68130.
Sanders KM, Akiyama T (2018) The vicious cycle of itch and anxiety. Neurosci Biobehav Rev 87:17–26.
Sanders KM, Sakai K, Henry TD, Hashimoto T, Akiyama T (2019) A subpopulation of amygdala neurons mediates the affective component of itch. J Neurosci 39:3345–3356.
Schwartz N, Temkin P, Jurado S, Lim BK, Heifets BD, Polepalli JS, Malenka RC (2014) Chronic pain. Decreased motivation during chronic pain requires long-term depression in the nucleus accumbens. Science 345:535–542.
Soares-Cunha C, Coimbra B, Sousa N, Rodrigues AJ (2016) Reappraising striatal D1- and D2-neurons in reward and aversion. Neurosci Biobehav Rev 68:370–386.
Stuber GD, Sparta DR, Stamatakis AM, van Leeuwen WA, Hardjoprajitno JE, Cho S, Tye KM, Kempadoo KA, Zhang F, Deisseroth K, Bonci A (2011) Excitatory transmission from the amygdala to nucleus accumbens facilitates reward seeking. Nature 475:377–380.
Stuber GD, Britt JP, Bonci A (2012) Optogenetic modulation of neural circuits that underlie reward seeking. Biol Psychiatry 71:1061–1067.
Su XY, Chen M, Yuan Y, Li Y, Guo SS, Luo HQ, Huang C, Sun W, Li Y, Zhu MX, Liu MG, Hu J, Xu TL (2019) Central processing of itch in the midbrain reward center. Neuron 102:858–872.e5. e855.
Suska A, Lee BR, Huang YH, Dong Y, Schlüter OM (2013) Selective presynaptic enhancement of the prefrontal cortex to nucleus accumbens pathway by cocaine. Proc Natl Acad Sci U S A 110:713–718.
Tejeda HA, Wu J, Kornspun AR, Pignatelli M, Kashtelyan V, Krashes MJ, Lowell BB, Carlezon WA Jr, Bonci A (2017) Pathway- and cell-specific kappa-opioid receptor modulation of excitation-inhibition balance differentially gates D1 and D2 accumbens neuron activity. Neuron 93:147–163.
Wang J, Ishikawa M, Yang Y, Otaka M, Kim JY, Gardner GR, Stefanik MT, Milovanovic M, Huang YH, Hell JW, Wolf ME, Schlüter OM, Dong Y (2018) Cascades of homeostatic dysregulation promote incubation of cocaine craving. J Neurosci 38:4316–4328.
Wang Y, Liu Z, Cai L, Guo R, Dong Y, Huang YH (2020) A critical role of basolateral amygdala-to-nucleus accumbens projection in sleep regulation of reward seeking. Biol Psychiatry 87:954–966.
Watabe-Uchida M, Zhu L, Ogawa SK, Vamanrao A, Uchida N (2012) Whole-brain mapping of direct inputs to midbrain dopamine neurons. Neuron 74:858–873.
Wikström B, Gellert R, Ladefoged SD, Danda Y, Akai M, Ide K, Ogasawara M, Kawashima Y, Ueno K, Mori A, Ueno Y (2005) Kappa-opioid system in uremic pruritus: multicenter, randomized, double-blind, placebo-controlled clinical studies. J Am Soc Nephrol 16:3742–3747.
Wu XB, Jing PB, Zhang ZJ, Cao DL, Gao MH, Jiang BC, Gao YJ (2018) Chemokine receptor CCR2 contributes to neuropathic pain and the associated depression via increasing NR2B-mediated currents in both D1 and D2 dopamine receptor-containing medium spiny neurons in the nucleus accumbens shell. Neuropsychopharmacology 43:2320–2330.
Wu ZH, Shao HY, Fu YY, Wu XB, Cao DL, Yan SX, Sha WL, Gao YJ, Zhang ZJ (2021) Descending modulation of spinal itch transmission by primary somatosensory cortex. Neurosci Bull 37:1345–1350.
Yang H, de Jong JW, Tak Y, Peck J, Bateup HS, Lammel S (2018) Nucleus accumbens subnuclei regulate motivated behavior via direct inhibition and disinhibition of VTA dopamine subpopulations. Neuron 97:434–449.e4.
Yuan L, Liang TY, Deng J, Sun YG (2018) Dynamics and functional role of dopaminergic neurons in the ventral tegmental area during itch processing. J Neurosci 38:9856–9869.
Yuan L, Dou YN, Sun YG (2019) Topography of reward and aversion encoding in the mesolimbic dopaminergic system. J Neurosci 39:6472–6481.
Zachariae R, Lei U, Haedersdal M, Zachariae C (2012) Itch severity and quality of life in patients with pruritus: preliminary validity of a Danish adaptation of the itch severity scale. Acta Derm Venereol 92:508–514.
Zahm DS, Brog JS (1992) On the significance of subterritories in the "accumbens" part of the rat ventral striatum. Neuroscience 50:751–767.
Zhang TT, Guo SS, Wang HY, Jing Q, Yi X, Hu ZH, Yu XR, Xu TL, Liu MG, Zhao X (2022) An anterior cingulate cortex-to-midbrain projection controls chronic itch in mice. Neurosci Bull. Advance online publication. Retrieved Dec 17, 2022. https://doi.org/10.1007/s12264-022-00996-6.
Zhang XY, Peng SY, Shen LP, Zhuang QX, Li B, Xie ST, Li QX, Shi MR, Ma TY, Zhang Q, Wang JJ, Zhu JN (2020) Targeting presynaptic H3 heteroreceptor in nucleus accumbens to improve anxiety and obsessive-compulsive-like behaviors. Proc Natl Acad Sci U S A 117:32155–32164.
Zhou H, Martinez E, Lin HH, Yang R, Dale JA, Liu K, Huang D, Wang J (2018) Inhibition of the prefrontal projection to the nucleus accumbens enhances pain sensitivity and affect. Front Cell Neurosci 12:240.